# Time and frequency resolved transient-absorption and stimulated-Raman signals of stochastic light

Cite as: J. Chem. Phys. **151**, 044113 (2019); https://doi.org/10.1063/1.5109258
Submitted: 07 May 2019 . Accepted: 27 June 2019 . Published Online: 30 July 2019

V. Al. Osipov, S. Asban, and S. Mukamel

The Journal of Chemical Physics

ARTICLE

scitation.org/journal/jcp

# Time and frequency resolved transient-absorption and stimulated-Raman signals of stochastic light

Cite as: J. Chem. Phys. 151, 044113 (2019); doi: 10.1063/1.5109258
Submitted: 7 May 2019 • Accepted: 27 June 2019 •
Published Online: 30 July 2019

View Online Export Citation CrossMark

**V. Al. Osipov, S. Asban, and S. Mukamel**[a)]

## AFFILIATIONS

Department of Chemistry and Department of Physics and Astronomy, University of California, Irvine, California 92697-2025, USA

**Note:** This paper is part of the JCP special collection on Ultrafast Spectroscopy and Diffraction from XUV to X-ray.
[a)] **Electronic mail:** muksec@uci.edu

## ABSTRACT

Covariance spectroscopy signals based on the transmission of broadband stochastic probe light undergoing a nonlinear optical process with matter are studied. The resulting signal depends on intensity correlation functions of the probe pulse. Application is made to transient absorption and stimulated Raman signals, where an ultraviolet pump and a delayed stochastically modulated infrared or optical Raman probe are used for monitoring vibrational excitations. We show that the stochastic properties of light can be exploited to circumvent the limitations on the joint temporal and spectral resolution of the signal. We study a model system with a time-dependent frequency and show that the dynamical information can be fully extracted from the covariance signal. This information is heavily suppressed upon averaging of noisy signals and practically inaccessible in conventional stimulated Raman measurements.

## I. INTRODUCTION

The effects of laser light incoherence on spectroscopic measurements have been studied since the early days of lasers in the 1970s.[1–4] Interest in the problem was motivated by the lack of ideal coherent laser sources, which made it hard to observe nonlinear optical effects in a controlled way. This continued to be the case until the development of coherent mode-locked lasers,[5] whose coherence time can reach hundreds of seconds. X-ray sources now face similar challenges, and stochastic models have been reviewed recently with applications to free electron x-ray lasers.[6–8]

In this article, we discuss the merits of combining the femtosecond pump-probe technique with stochastically modulated light. The pump-probe technique is commonly used in the study of photoinduced processes in molecular systems.[9] The pump induces optical transitions, which are then detected by the probe at different frequency regimes [infrared (IR), ultraviolet (UV), or X-rays]. The effective temporal and spectral resolution of the UV/IR pulse is not determined solely by its control parameters but depends on the studied system. The frequency resolution of a spectrometer and the time-frequency uncertainty of light can be varied independently. However, ultrafast resolution of the signal requires the active involvement of the entire probe bandwidth, while in a given application, the system may select a narrower segment of the pulse.[10–12] Simultaneous high spectral and temporal resolution cannot be realized in transient absorption, where the signal involves two interactions with the probe, that determines both the temporal and spectral resolutions. One approach to manipulate the joint spectral and temporal resolution is via chirped pulses.[13–16] The chirped probe pulse has a time-frequency profile, which can be described by the rotation of a narrowband pulse in time-frequency space, so that the pulse may be viewed as a combination of waves with different frequencies and distributed arrival times. This allows us to extend the probe-pulse envelope in both the frequency and time domains.

In this paper, we use a covariance analysis of the transient absorption signal generated by a stochastically modulated probe pulse. Rather than controlling the temporal and spectral properties of a fluctuating probe field, we propose control of its statistical properties.[17] Rapid decay of the correlation function translates into a phase matching, and the correlations in the stochastic light field allow us to single out desired time/frequency intervals. Correlation functions are accessible experimentally through ensemble averaging over realizations of repeated measurements. In Ref. 18, it has been shown that the covariance spectroscopy approach can be extended for investigation of two-dimensional electronic spectra and allows us to increase the method sensitivity to long-lived intermediates. We demonstrate that covariance spectroscopy with a stochastic probe makes it possible to achieve joint high temporal and spectral resolution and can be used for monitoring fast dynamical changes in molecular systems. The method can also be applied to other noisy sources such as free electron lasers, based on self-amplified spontaneous emission (SASE).[19,20]

The experimental setup of time-resolved transmitted light spectroscopy starts with a visible or UV (actinic) pulse, which launches some electronic or nuclear dynamics in the molecule. We then consider two detection schemes: (i) Transient absorption (TA): An intense near-infrared broadband probe pulse arrives after a time delay $T$. The probe frequency-dispersed transmission is observed for various values of $T$; see Fig. 1(a). (ii) Stimulated Raman spectroscopy (SRS) [Fig. 4(a)]: A combined narrowband and broadband probe is used to generate a Raman process.

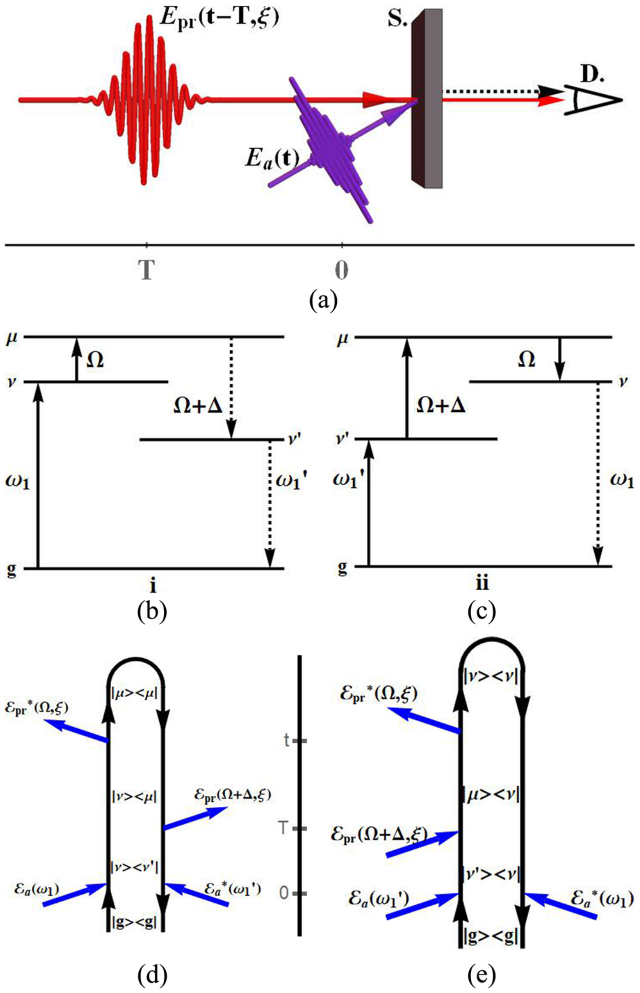

**FIG. 1**. (a) Schematic layout of the TA setup. The actinic pulse $E_a$ excites the sample (S.) at time $t = 0$ and prepares it in the superposition $|\nu\rangle\langle\nu'|$, the stochastic probe pulse arrives at time $T$, and the transmitted light is measured by detector (D.) at time $t$; level schemes [(b) and (c)] and loop diagrams [(d) and (e)] contributing to TA signal, $\xi$ is the stochastic phase.

The UV/IR TA signal may be viewed as a sequence of four events: An IR actinic pump impulsively creates vibrational coherence. The system then interacts twice with the probe field which results in almost instantaneous excitation and deexcitation to one of vibrational levels. We assume that each frequency of the probe pulse is modulated by a random phase. The ensemble-averaged TA signal, calculated in Sec. II A when the probe field is modulated by almost uncorrelated random phases, is weak. In contrast, the second-order intensity correlation function yields the covariance signal, which survives the averaging and contains information about the molecular transitions. The formal definition of the TA covariance signal is defined in Sec. II. This signal is simulated in Sec. II C for $\delta$-correlated random phases (i.e., random phase modulation at each frequency is statistically independent from modulated phases at other frequencies), and the covariance spectrogram is analyzed. The spectrogram for finitely correlated phases is discussed as well. The SRS covariance signal is derived and simulated in Sec. III. In Sec. IV, a model of open molecular system with a time-dependent vibrational frequency is studied. We develop a method, which allows us to reveal the time-flow of the molecular system dynamics from the covariance spectroscopy.

## II. THE TRANSIENT ABSORPTION COVARIANCE SIGNAL

TA is a pump-probe technique[9,21–25] that usually employs a UV probe and near-IR broadband probe pulse. The measurement is performed by varying the delay $T$ between the pulses and detecting the transmission change in the probe by interaction with matter; see Fig. 1(a). In covariance spectroscopy, each frequency of the broadband probe pulse is additionally modulated by a frequency-dispersed random phase $\xi(\omega)$,

$$\mathcal{E}_{pr}(\omega,\xi) = \bar{\mathcal{E}}_{pr}(\omega)e^{i\xi(\omega)}. \qquad (1)$$

Here, $\mathcal{E}(\omega)$ is the Fourier transform of the electric field $E(t)$. The ensemble is sampled by many repetitions of the experiment with various realizations of the fluctuating phase.

The Hamiltonian of the system is $H = H_0 + H_{int}$, where $H_0 = \sum_\nu \hbar\omega_\nu |\nu\rangle\langle\nu|$ is the unperturbed molecular Hamiltonian with excitation energies $\omega_\nu$ and eigenstates $|\nu\rangle$. The light-matter interaction in the rotating-wave approximations is given by

$$H_{int} = \hbar\hat{V}^\dagger\hat{E}(t) + h.c., \qquad (2)$$

where $\hbar\hat{V}^\dagger$ is the raising dipole operator. The positive frequency component of the electric field is given by the sum of the actinic pulse field and the stochastic probe pulse,

$$\hat{E}(t) = E_a(t) + E_{pr}(t-T,\xi). \qquad (3)$$

The frequency-gated TA signal, $\mathscr{S}_{TA,\xi}(\Omega,T)$, generated by the stochastic light field [Eq. (1)], is[12]

$$\mathscr{S}_{TA,\xi}(\Omega,T) = 2\Im\, \mathscr{E}^*_{pr}(\Omega,\xi)\int_{-\infty}^{\infty}\frac{d\Delta}{2\pi}\mathscr{E}_{pr}(\Omega+\Delta,\xi)\bar{\mathrm{S}}(\Omega,T;\Delta). \quad (4)$$

The auxiliary signal, $\bar{\mathrm{S}}(\Omega,T;\Delta)$, can be read off the loop diagrams shown in Fig. 1(b),

$$\bar{\mathrm{S}}(\Omega,T;\Delta) = \bar{\mathrm{S}}_{TA(i)}(\Omega,T;\Delta) + \bar{\mathrm{S}}_{TA(ii)}(\Omega,T;\Delta), \quad (5)$$

where

$$\begin{aligned}\bar{\mathrm{S}}_{TA(i)}&(\Omega,T;\Delta)\\ &= 2\mathrm{i}\hbar^3 e^{\mathrm{i}\Delta T}\int_{-\infty}^{\infty}\frac{d\omega_1}{2\pi}\frac{d\omega_1'}{2\pi}\mathscr{E}_a(\omega_1)\mathscr{E}_a^*(\omega_1')\delta(\omega_1-\omega_1'+\Delta)\\ &\quad\times\langle\hat{V}\tilde{G}^\dagger(\omega_1')\hat{V}^\dagger\tilde{G}^\dagger(\omega_1'-\Omega-\Delta)\hat{V}\tilde{G}(\omega_1)\hat{V}^\dagger\rangle, \quad (6)\end{aligned}$$

$$\begin{aligned}\bar{\mathrm{S}}_{TA(ii)}&(\Omega,T;\Delta)\\ &= 2\mathrm{i}\hbar^3 e^{\mathrm{i}\Delta T}\int_{-\infty}^{\infty}\frac{d\omega_1}{2\pi}\frac{d\omega_1'}{2\pi}\mathscr{E}_a(\omega_1')\mathscr{E}_a^*(\omega_1)\delta(\omega_1'-\omega_1+\Delta)\\ &\quad\times\langle\hat{V}\tilde{G}^\dagger(\omega_1)\hat{V}\tilde{G}(\omega_1'+\Omega+\Delta)\hat{V}^\dagger\tilde{G}(\omega_1')\hat{V}^\dagger\rangle. \quad (7)\end{aligned}$$

The $\delta$-function in the integrand guarantees energy conservation, and $\tilde{G}(\omega)$ is Green's function of free molecular propagation.

Covariance signals are obtained by data processing of the transmitted stochastic probe pulse. We focus on the covariance of the detected light intensity at two frequencies,

$$C(\Omega_1,\Omega_2) = \frac{\langle\mathscr{S}_\xi(\Omega_1,T)\mathscr{S}_\xi(\Omega_2,T)\rangle_\xi - \langle\mathscr{S}_\xi(\Omega_1,T)\rangle_\xi\langle\mathscr{S}_\xi(\Omega_2,T)\rangle_\xi}{\sqrt{\langle\mathscr{S}^2_\xi(\Omega_1,T)\rangle_\xi\,\langle\mathscr{S}^2_\xi(\Omega_2,T)\rangle_\xi}}, \quad (8)$$

where the brackets $\langle\,\cdot\,\rangle_\xi$ denote averaging over the ensemble of realizations of the random function $\xi(\omega)$.

The covariance (8) depends on the expectation values $\langle\mathscr{S}_\xi(\Omega,T)\rangle_\xi$ and $\langle\mathscr{S}_\xi(\Omega_1,T)\mathscr{S}_\xi(\Omega_2,T)\rangle_\xi$. The ensemble-averaged signal [Eq. (4)] is given by

$$\langle\mathscr{S}_\xi(\Omega,T)\rangle_\xi = 2\Im\,\bar{\mathscr{E}}^*_{pr}(\Omega)\int_{-\infty}^{\infty}\frac{d\Delta}{2\pi}\bar{\mathscr{E}}_{pr}(\Omega+\Delta)\mathscr{N}(\Delta)\bar{\mathrm{S}}(\Omega,T;\Delta), \quad (9)$$

where the role of stochasticity is contained in the autocorrelation function,

$$\mathscr{N}(\Delta) \equiv \langle e^{\mathrm{i}\xi(\Omega+\Delta)-\mathrm{i}\xi(\Omega)}\rangle_\xi. \quad (10)$$

The correlation function of the signal (4) can be calculated with the help of the identity $\Im\,a\cdot\Im\,b = \frac{1}{2}\Re\big(ab^*-ab\big)$,

$$\begin{aligned}\langle\mathscr{S}_\xi(\Omega_1,T)\mathscr{S}_\xi(\Omega_2,T)\rangle_\xi - \langle\mathscr{S}_\xi(\Omega_1,T)\rangle_\xi\langle\mathscr{S}_\xi(\Omega_2,T)\rangle_\xi &= 2\Re\int_{-\infty}^{\infty}\frac{d\Delta_1}{2\pi}\bar{\mathscr{E}}^*_{pr}(\Omega_1)\bar{\mathscr{E}}_{pr}(\Omega_1+\Delta_1)\,\bar{\mathrm{S}}(\Omega_1,T;\Delta_1)\int_{-\infty}^{\infty}\frac{d\Delta_2}{2\pi}\\ &\quad\times\Big[\bar{\mathscr{E}}_{pr}(\Omega_2)\bar{\mathscr{E}}^*_{pr}(\Omega_2+\Delta_2)\bar{\mathrm{S}}^*(\Omega_2,T;\Delta_2)[\Xi(\Omega_1,\Omega_2+\Delta_2,\Delta_1,-\Delta_2)-\mathscr{N}(\Delta_1)\mathscr{N}(\Delta_2)]\\ &\quad-\bar{\mathscr{E}}^*_{pr}(\Omega_2)\bar{\mathscr{E}}_{pr}(\Omega_2+\Delta_2)\bar{\mathrm{S}}(\Omega_2,T;\Delta_2)\big[\Xi\big(\Omega_1,\Omega_2,\Delta_1,\Delta_2\big)-\mathscr{N}(\Delta_1)\mathscr{N}(\Delta_2)\big]\Big], \quad (11)\end{aligned}$$

where $\Xi$ is the four-point correlation function,

$$\Xi(\Omega_1,\Omega_2,\Delta_1,\Delta_2) \equiv \langle e^{\mathrm{i}\xi(\Omega_1+\Delta_1)-\mathrm{i}\xi(\Omega_1)+\mathrm{i}\xi(\Omega_2+\Delta_2)-\mathrm{i}\xi(\Omega_2)}\rangle_\xi. \quad (12)$$

Until now, we made no assumptions about the type of noise. The choice of particular model is dictated by experimental details. Nevertheless, we can formulate a number of generic requirements: (i) Since the material object of investigation is a molecule, whose size is usually assumed to be much smaller than the radiation wavelength, any possible spatial decoherence of light plays no role in our consideration. (ii) To characterize the temporal/frequency randomness of the light field, it is enough to define the correlation functions in one of the two domains, either in frequency domain or in time domain. In our model, the probe field is represented by a sum of strongly localized pulses with statistically independent random phases $\xi(\omega)$ and deterministic envelop function $\bar{\mathscr{E}}_{pr}(\omega)$. This pulse structure requires fast decay of the correlation functions [Eqs. (10) and (12)] with respect to the arguments $\Delta$, $\Delta_1$, and $\Delta_2$. The higher order correlation functions have the same property, but they are not used in further calculations. In Sec. II A, we consider a particular mathematical model of the noise.

### A. The averaged signal for the Brownian phase model

In this model,[17,26–28] the random phase $\xi(\omega)$ is taken to be a one-dimensional Brownian coordinate, which varies along the $\omega$ axis. The phase increment $|\xi(\Omega+\Delta)-\xi(\Omega)|$ is independent of $\Omega$ and has a Gaussian distribution, whose variance grows linearly with the interval length, $\langle\big(\xi(\Omega+\Delta)-\xi(\Omega)\big)^2\rangle_\xi = \mathscr{T}_C|\Delta|$, where $\mathscr{T}_C$ is autocorrelation time. For this model, $\mathscr{N}(\Delta) = e^{-|\Delta|\mathscr{T}_C}$ and $\Xi$ [Eq. (12)] is given in Appendix A and is displayed in Fig. 10. Equation (9) now reads

$$\begin{aligned}\langle\mathscr{S}_\xi&(\Omega,T)\rangle_\xi\\ &= \int_{-\infty}^{\infty}\frac{d\kappa}{2\pi\mathscr{T}_C}\left[\frac{1}{1+\mathrm{i}(\kappa-T)/\mathscr{T}_C}+\frac{1}{1-\mathrm{i}(\kappa-T)/\mathscr{T}_C}\right]\mathscr{W}(\Omega,\kappa), \quad (13)\end{aligned}$$

where

$$\mathscr{W}(\Omega,\kappa) = 2\Im\, \bar{\mathscr{E}}^{*}_{pr}(\Omega) \int_{-\infty}^{\infty} \frac{d\Delta}{2\pi} \bar{\mathscr{E}}_{pr}(\Omega+\Delta)\bar{\mathrm{S}}(\Omega,\kappa;\Delta). \tag{14}$$

The averaged signal is given by a convolution of the auxiliary signal $\mathscr{W}(\Omega,\kappa)$ with a Lorentzian kernel. The auxiliary signal (14) is given by Eq. (4) but is calculated for the deterministic probe pulse, $\bar{\mathscr{E}}_{pr}(\omega)$, and at time $\kappa$ (different from $T$). The spreading of the interval $T - \kappa$ reduces the temporal resolution and is governed by the correlation time $\mathscr{T}_C$. For strongly correlated phases, i.e., when $\mathscr{T}_C \to 0$ $\mathscr{W}(\Omega, T) \equiv \mathscr{S}(\Omega, T)$, so that Eqs. (13) and (14) recover the signal (4). The $1/\mathscr{T}_C$ factor in Eq. (15) implies that decoherence (loss of phase memory) reduces the average signal magnitude. For finite $\mathscr{T}_C$, only the time interval of length ~ $\mathscr{T}_C$ in the vicinity of $T$ contributes to the integral in Eq. (13). Narrowing this interval weakens the average signal. In the limit of $\delta$-correlated phases, $\langle\xi(\Omega)\xi(\Omega+\Delta)\rangle_\xi = \delta(\Delta)$. When $\mathscr{T}_C \to \infty$, Eqs. (13) and (14) result in the averaged TA signal,

$$\langle\mathscr{S}_\xi(\Omega,T)\rangle_\xi \propto \frac{2\left|\bar{\mathscr{E}}_{pr}(\Omega)\right|^2}{\mathscr{T}_C}\Im\,\bar{\mathrm{S}}(\Omega,T;0). \tag{15}$$

Note that Eq. (15) is independent of $T$ since $T$ enters $\bar{\mathrm{S}}(\Omega,\kappa;\Delta)$ only through the phase $e^{\mathrm{i}\Delta T}$ [see Eqs. (6) and (7)]. The $1/\mathscr{T}_C$ factor in Eq. (15) implies that the average signal becomes weak for short-range phase correlations. Nevertheless, the information can be retrieved from the covariance signal, which remains finite, as shown below.

### B. Covariance signal for the Brownian phase model

For the model of Brownian random phase $\xi(\omega)$, introduced in Sec. II A (see also Appendix A), the four-point correlation function $\Xi(\Omega_1, \Omega_2, \Delta_1, \Delta_2)$ [Eq. (A2)] shown in Fig. 10(a) has two sharp maxima at the following points:

$$\Delta_1 = \Delta_2 = 0, \tag{16}$$

$$\Delta_1 = -\Delta_2 = \Omega_2 - \Omega_1, \qquad \Omega_2 \neq \Omega_1, \tag{17}$$

and decays exponentially on the $\mathscr{T}_C$ scale. This rapid decay makes it possible to evaluate the covariance off-diagonal terms using the saddle-point approximation. Assuming $|\Omega_1 - \Omega_2|\mathscr{T}_C \gg 1$ and that the maxima of $\Xi(\Omega_1, \Omega_2, \Delta_1, \Delta_2)$ are well separated, we obtain for the covariance signal at $\Omega_1 \neq \Omega_2$

$$C(\Omega_1,\Omega_2) \simeq -\frac{1}{\sqrt{\mathscr{I}(\Omega_1)\mathscr{I}(\Omega_2)}}\Re\int_{-\infty}^{\infty}\frac{d\kappa_1}{2\pi}\int_{-\infty}^{\infty}\frac{d\kappa_2}{2\pi} \times \frac{\mathscr{W}(\Omega_1,\kappa_1)\mathscr{W}(\Omega_2,\kappa_2)e^{\mathrm{i}(\Omega_1-\Omega_2)(\kappa_1-\kappa_2)}}{\left(1+(\kappa_1-T)^2/(2\mathscr{T}_C^2)+(\kappa_2-T)^2/(2\mathscr{T}_C^2)\right)^{3/2}}, \tag{18}$$

where $\mathscr{W}(\Omega,\kappa)$ is given by Eq. (14), and

$$\mathscr{I}(\Omega) = \int_{-\infty}^{\infty} d\Delta\left|\bar{\mathscr{E}}_{pr}(\Omega)\bar{\mathscr{E}}_{pr}(\Omega+\Delta)\bar{\mathrm{S}}(\Omega,T;\Delta)\right|^2. \tag{19}$$

Equation (18) gives the covariance for long $\mathscr{T}_C$. In the other extreme $\mathscr{T}_C \to 0$ (infinitely correlated phases), the correlation functions $\mathscr{N}(\Delta)$ and $\Xi(\Omega_1, \Omega_2, \Delta_1, \Delta_2)$ tend to one so that the covariance $\langle\mathscr{S}_\xi(\Omega_1,T)\mathscr{S}_\xi(\Omega_2,T)\rangle_\xi - \langle\mathscr{S}_\xi(\Omega_1,T)\rangle_\xi\langle\mathscr{S}_\xi(\Omega_2,T)\rangle_\xi$ vanishes at all $\Omega_1 \neq \Omega_2$; see Eq. (11).

For $\delta$-correlated phases, $\mathscr{T}_C \to \infty$. Using the representation $\delta(x) = \frac{1}{2}\lim_{\mathscr{T}_C\to\infty}\mathscr{T}_C e^{-|x|\mathscr{T}_C}$, the function $\Xi$ becomes

$$\lim_{\mathscr{T}_C\to\infty}(\mathscr{T}_C/2)\cdot\Xi(\Omega_1,\Omega_2,\Delta_1,\Delta_2) = \delta(\Delta_1)\delta(\Delta_2) + \delta(\Omega_1-\Omega_2+\Delta_1)\delta(\Omega_1-\Omega_2-\Delta_2). \tag{20}$$

The first term cancels with the product $\langle\mathscr{S}_\xi(\Omega_1;T)\rangle_\xi\langle\mathscr{S}_\xi(\Omega_2;T)\rangle_\xi$ upon substitution into Eq. (8), and the second product of $\delta$-functions gives

$$C(\Omega_1,\Omega_2) = \delta(\Omega_2-\Omega_1)\frac{\mathscr{I}(\Omega_1)-\Re\bar{\mathrm{S}}^2(\Omega_1,T;0)}{\sqrt{\mathscr{I}(\Omega_1)\mathscr{I}(\Omega_2)}} - \left|\bar{\mathscr{E}}_{pr}(\Omega_1)\right|^2\left|\bar{\mathscr{E}}_{pr}(\Omega_2)\right|^2 \times \frac{\Re\bar{\mathrm{S}}(\Omega_1,T;\Omega_2-\Omega_1)\bar{\mathrm{S}}(\Omega_2,T;\Omega_1-\Omega_2)}{\sqrt{\mathscr{I}(\Omega_1)\mathscr{I}(\Omega_2)}}. \tag{21}$$

The same result can be obtained from Eq. (18) for $\mathscr{T}_C \to \infty$. When $\mathscr{T}_C$ is long, the denominator in the integrand of Eq. (18) can be replaced by a constant, and the $\kappa_1$ and $\kappa_2$ integrals yield the product $\delta(\Delta_1 + \Omega_1 - \Omega_2)\delta(\Delta_2 - \Omega_1 + \Omega_2)$, where $\Delta_1$ and $\Delta_2$ are the integration variables in Eq. (14). We then recover Eq. (21). In this limit, the phase correlations are narrower than all decoherence rates. Note that despite $T$ dependence of the auxiliary signal $\bar{\mathrm{S}}(\Omega_1, T; \Omega_2 - \Omega_1)$, the resulting expression (21) in this limit is independent of $T$. This becomes clear upon the substitution of Eqs. (6) and (7) into Eq. (21). In this limit, the probe pulse temporal envelope is infinitely large and the $T$ parameter may no longer be observed. For finite $\mathscr{T}_C$, the integration order in Eq. (18) must be kept resulting in increased line widths in the covariance spectrum. This limit is discussed in more detail in Sec. II C.

To conclude, $\mathscr{T}_C$ controls the time and frequency dispersion of the probe pulse. Variation of $\mathscr{T}_C$ allows us to resolve resonances with a short lifetime (compared to $\mathscr{T}_C$) and can blur the long-living resonances. The natural constrains for $\mathscr{T}_C$ are the time-interval separating the actinic and probe pulses, and the lifetime of the system's state. The averaged signal is a convolution of the signal [Eq. (13)] calculated with deterministic amplitude of the probe pulse taken at various moments of the arrival time $\kappa$ [Eq. (14)]. Variable $\kappa$ in Eqs. (13) and (14) plays a role of a new arrival time of the pulse. The same structure has Eq. (21) for the covariance signal, where now the deterministic signals at two different $\kappa_1$ and $\kappa_2$ are convoluted.

### C. Simulations of the transient absorption covariance signal

We first consider the TA signal simulated for a three electronic level $|g\rangle$, $|e\rangle$, and $|f\rangle$ model system, where the state $|e\rangle$ supports three vibrational levels $|e\rangle$, $|e'\rangle$, and $|e''\rangle$, as shown in Fig. 2(a). Assuming that the actinic pulse is impulsive ($E_a(t) = \mathscr{E}_a\delta(t)$), the TA auxiliary signal (see details in Appendix B) can be calculated using Eqs. (B5) and (B6) to give

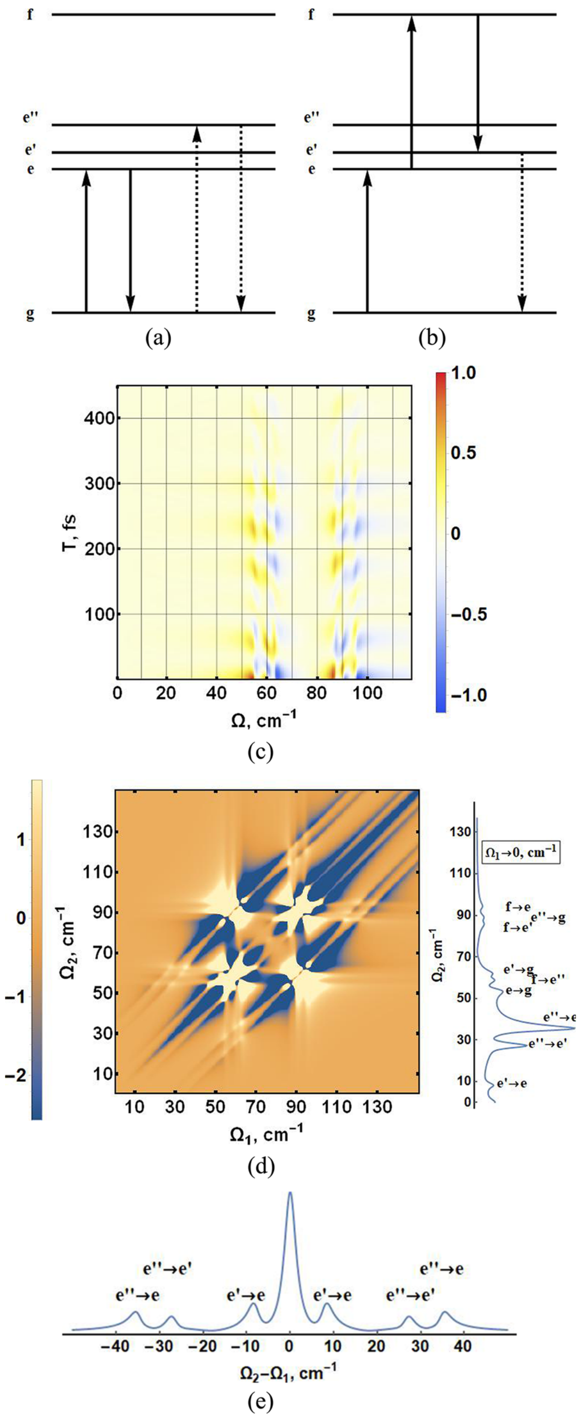

**FIG. 2**. Panels (a) and (b) depict the two quantum pathways contributing to the TA signal [Eq. (23)] shown by arrows; (c) the TA signal simulated for a three electronic level system; (d) the simulated TA covariance signal. Parameters of the model are $\omega_g$ = 770 cm$^{-1}$, $\omega_e$ = 825 cm$^{-1}$, $\omega_{e'}$ = 835 cm$^{-1}$, $\omega_{e''}$ = 860 cm$^{-1}$, and $\omega_f$ = 920 cm$^{-1}$; all decoherence rates $\varepsilon$ are equal to 60 ps, $|\bar{\mathscr{E}}_{pr}| = |\mathscr{E}_a| = 1$, and all transition dipole moments are equal to one. (e) Cross section of the covariance spectra along the diagonal $\Omega_1 + \Omega_2$ = 50 cm$^{-1}$.

$$\bar{S}_{TA}(\Omega, T; \Delta) = 2|\mathscr{E}_a|^2 \sum_{\nu,\nu'=e,e',e''} \nu_{g,\nu}\nu^*_{\nu',g} \sum_{\mu=f,g} \nu_{\mu,\nu'}\nu^*_{\nu,\mu} \frac{e^{\mathrm{i}\Delta T}}{\omega_{\nu',\nu} + \Delta - \mathrm{i}\varepsilon_{\nu',\nu}} \times \left[\frac{1}{\omega_{\nu',\mu} - \Omega - \mathrm{i}\varepsilon_{\nu',\mu}} - \frac{1}{\omega_{\nu,\mu} + \Omega + \mathrm{i}\varepsilon_{\nu,\mu}}\right], \tag{22}$$

where $\varepsilon_{\nu,\mu}$ are the decoherence rates and $\omega_{\mu,\nu}$ denotes the excitation energies, $\omega_{\mu,g} - \omega_{\nu,g}$. The complex coefficients $\nu_{\nu,\mu}$ are matrix elements of the transition dipole operators $\hat{V}$. Only transitions between electronic levels ($g \leftrightarrows e, e', e'' \leftrightarrows f$) are allowed in our model, and its parameters are given in the caption of Fig. 2.

The TA signal generated by an impulsive deterministic probe pulse, i.e., $E_{pr}(t, \xi) = \bar{\mathscr{E}}_{pr} e^{-\mathrm{i}\omega_{pr}T}\delta(t-T)$ and $\xi(\omega) = 0$, can be obtained from Eq. (22) by using Eq. (4),

$$\mathscr{S}_{TA}(\Omega, T) = 2|\mathscr{E}_a|^2 |\bar{\mathscr{E}}_{pr}|^2 \Re \sum_{\nu,\nu'=e,e',e''} \nu_{g,\nu}\nu^*_{\nu',g} \sum_{\mu=f,g} \nu_{\mu,\nu'}\nu^*_{\nu,\mu} \times e^{-\mathrm{i}\omega_{\nu',\nu}T - \varepsilon_{\nu',\nu}T} \left[\frac{1}{\omega_{\nu',\mu} - \Omega - \mathrm{i}\varepsilon_{\nu',\mu}} - \frac{1}{\omega_{\nu,\mu} + \Omega + \mathrm{i}\varepsilon_{\nu,\mu}}\right]. \tag{23}$$

Equation (23) plotted in Fig. 2(c) vs $\Omega$ and $T$ shows six oscillating vertical lines at frequencies corresponding to the intervalence resonance excitations $\omega_{e,g}$ and $\omega_{f,g}$. The oscillation frequencies are given by the vibrational manifold frequencies $\omega_{e',e}$, $\omega_{e'',e'}$, and $\omega_{e'',e}$. The signal further contains nonoscillatory components which correspond to interaction pathways without energy absorption, such as $g \to e \to f \to e \to g$. The oscillations of the signal in $T$ can interfere, which complicates their resolution. The TA signal calculated for the system by excluding level $e'$ (i.e., transitions to this level are forbidden, $\nu_{g,e'} = \nu_{f,e'} = 0$) is plotted in Fig. 3(b). We only see a single oscillation frequency $\omega_{e'',e} = 35$ cm$^{-1}$.

Resolving desired features in the signal requires a transformation, which would amplify specific contributions to the signal. Fourier transform of $\mathscr{S}_{TA}(\Omega, T)$ with respect to $T$ is a linear unitary transformation. A different type of transformation is provided by the covariance signal. It is a quadratic transformation involving an integration over a given probability measure. The TA covariance signal for $\delta$-correlated phases and an impulsive deterministic envelope of the probe pulse can be calculated using Eq. (21). Diagonal features of the covariance carry no interesting information; we therefore focus on the off-diagonal features. These are expressed through the auxiliary signal [Eq. (22)] and up to a sign and normalization give

$$C_{TA}(\Omega_1, \Omega_2) \propto |\bar{\mathscr{E}}_{pr}|^4 \Re\, \bar{S}_{TA}(\Omega_1, T; \Omega_2 - \Omega_1)\bar{S}_{TA}(\Omega_2, T; \Omega_1 - \Omega_2). \tag{24}$$

We next examine the 2D covariance spectrum of the model system shown in Figs. 2(a) and 2(b) calculated for $\delta$-correlated phases using Eqs. (24) and (22). The model parameters are given in the caption of Fig. 2. The covariance spectrogram shown in Fig. 2(d) contains a pattern of horizontal, vertical, and diagonal lines and is symmetric with respect to the main diagonal, $\Omega_1 = \Omega_2$. This pattern is typical for covariance spectra[8,17] and can be interpreted using Eqs. (22) and (24). Each pathway contributing to the transient absorption process gives a product of two Lorentzians in the auxiliary signal $S_{TA}(\Omega, T; \Delta)$ [Eq. (22)]. The peaks in $\Omega$ describe resonances caused by transitions between electronic levels, while

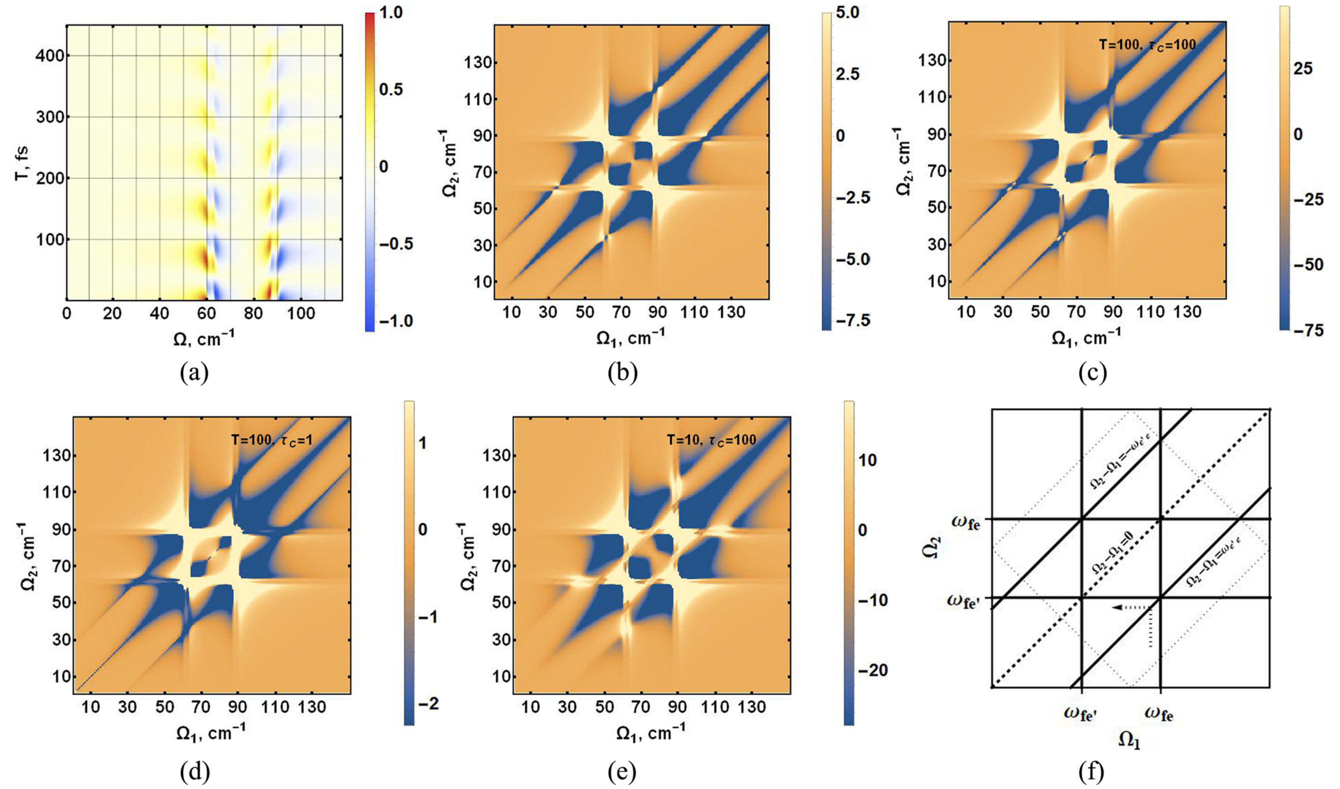

(a) (b) (c) (d) (e) (f)

**FIG. 3**. (a) TA signal [Eq. (23)]; (b) TA covariance signal [Eq. (24)] from the probe pulse with $\delta$-correlated phases; (c)–(e) TA covariance signals simulated for various combinations of $T$ and $\mathscr{T}_C$ (the values in fs are shown inside the plots). The plots are simulated for a two level model and a single vibrational level; see the level scheme in Fig. 2(a) with an excluded level $e''$ ($\nu_{g,e''} = \nu_{f,e''} = 0$); other parameters are $\omega_g$ = 770 cm$^{-1}$, $\omega_e$ = 825 cm$^{-1}$, $\omega_{e'}$ = 860 cm$^{-1}$, and $\omega_f$ = 920 cm$^{-1}$; the decoherence rates $\varepsilon$ are equal to 60 ps, $|\mathscr{E}_{pr}| = |\mathscr{E}_a| = 1$, and all nonzero transition dipole moments are equal to one; (f) the scheme of lines for 2D covariance spectrum for $\delta$-correlated phases [Eq. (21)]. The thick solid lines correspond to resonant maxima auxiliary signal $\bar{S}(\Omega_2, T; \Omega_1 - \Omega_2)$; the dashed line marks the diagonal $\Omega_2 = \Omega_1$. Intersection of three lines detects the excited state absorption process $e \to f \to g'$; see Fig. 2(b).

$\Delta$ is responsible for resonances between vibrational levels. For our model system with three vibrational levels, the spectrogram has three diagonal lines (from both sides of the main diagonal) and six vertical (horizontal) lines, which reveal the valence transition frequencies ($\omega_{e,g}$ = 55 cm$^{-1}$, $\omega_{e',g}$ = 65 cm$^{-1}$ $\omega_{e'',g}$ = 90 cm$^{-1}$, and $\omega_{f,e}$ = 95 cm$^{-1}$, $\omega_{f,e'}$ = 85 cm$^{-1}$ $\omega_{f,e''}$ = 60 cm$^{-1}$). The distances between the main diagonal and other diagonal lines correspond to the vibrational spacings $\omega_{e',e}$ = 10 cm$^{-1}$, $\omega_{e'',e'}$ = 25 cm$^{-1}$, and $\omega_{e'',e}$ = 35 cm$^{-1}$. All lines corresponding to absorption and emission of the same photon (for instance, the pathway $g \to e \to f \to e \to g$) overlap with the main diagonal and are not resolved by the covariance signal. The intersection points of three lines correspond to a particular quantum pathway describing absorption (emission) process of the transmitted light by the higher (lower) lying vibration level; see Fig. 3(f).

We have further investigated the influence of finite phase correlation range for the same model system with electronic levels $|e\rangle$ and $|f\rangle$, where level $|e\rangle$ has a single vibrational level $|e'\rangle$ (level $|e''\rangle$ is omitted). The bare TA signal [Eq. (23)] is given in Fig. 3(a). The TA covariance spectra displayed in Fig. 3 are calculated for a finite phase correlation length $1/\mathscr{T}_C$ using Eq. (18). Each spectrum has a single diagonal line (two lines symmetric with respect to the main diagonal), which corresponds to the vibrational frequency $\omega_{e',e}$ = 35 cm$^{-1}$ [compare panels (c) and (d) in Fig. 2 with panels (a) and (b) in Fig. 3]. In the covariance spectrogram generated by a probe with $\delta$-correlated phases [panel (b) in Fig. 3], the line shapes and their visible lengths are completely determined by the decoherence rates $\varepsilon$. The line shapes in the spectrograms generated for correlated phases depend on two temporal parameters: $T$ and $\mathscr{T}_C$. Panels (c), (d), and (e) in Fig. 3 show that this dependence is not strong. The overall pattern of the spectrogram remains virtually the same for various combinations of parameters $T$ and $\mathscr{T}_C$. More detailed analysis of the spectra shows that the decrease in $\mathscr{T}_C$ blurs the line shapes. For instance, for $\mathscr{T}_C > T$, the experimental time window cannot cover the entire probe pulse time-profile, which effectively changes the correlation time and makes it much weaker than the initial $\mathscr{T}_C$. Such an effective change in $\mathscr{T}_C$ is reflected in shorter but broader diagonal lines in the spectrogram [compare plots (c) and (e) in Fig. 3].

To conclude, we note that the finite correlation range of random phases does not influence the spectrum significantly. The pattern contains well resolved lines for reasonable combinations of $T$ and $\mathscr{T}_C$ so that the desired spectroscopic information can be extracted from the covariance spectrum.

## III. THE STIMULATED RAMAN SPECTROSCOPIC COVARIANCE SIGNAL

We next turn to stimulated Raman spectroscopy which is a common technique for probing time-resolved vibrational dynamics.[10,11,14,29–32] In this experiment, nuclear dynamics in an excited electronic state launched by the actinic pulse ($E_a$) is subsequently probed by a combination of a narrow ($E_2$)- and broad ($E_{pr}$)-band pulse arriving simultaneously at time $T$; see Fig. 4(a). The carrier frequency of $E_2$ is tuned to a selected resonance with the transition between single and double excited electronic levels, to generate fast resonant Raman transitions in the system. The pulses propagate in different directions determined by wave-vectors $\boldsymbol{k}_1$, $\boldsymbol{k}_2$, and $\boldsymbol{k}_3$. The transmitted broadband pulse is frequency dispersed and detected along $\boldsymbol{k}_3$.

In covariance SRS, the probe pulse is modulated by a random phase, $\xi$. The positive frequency component of the electric field is given by the sum of three fields,

$$E(t) = E_a(t)e^{\mathrm{i}\boldsymbol{k}_1\boldsymbol{r}} + E_2(t-T)e^{\mathrm{i}\boldsymbol{k}_2\boldsymbol{r}} + E_{pr}(t-T,\xi)e^{\mathrm{i}\boldsymbol{k}_3\boldsymbol{r}}. \tag{25}$$

The light-matter interaction is given by the dipole Hamiltonian in the rotating wave approximation [Eq. (2)]. In analogy with TA [Eq. (4)], the SRS signal can be represented by the convolution

$$\mathscr{S}_{SRS,\xi}(\Omega,T) = 2\Im\, \mathscr{E}^*_{pr}(\Omega,\xi)\int_{-\infty}^{\infty}\frac{d\Delta}{2\pi}\mathscr{E}_{pr}(\Omega+\Delta,\xi)\bar{\mathrm{S}}_{SRS}(\Omega,T;\Delta). \tag{26}$$

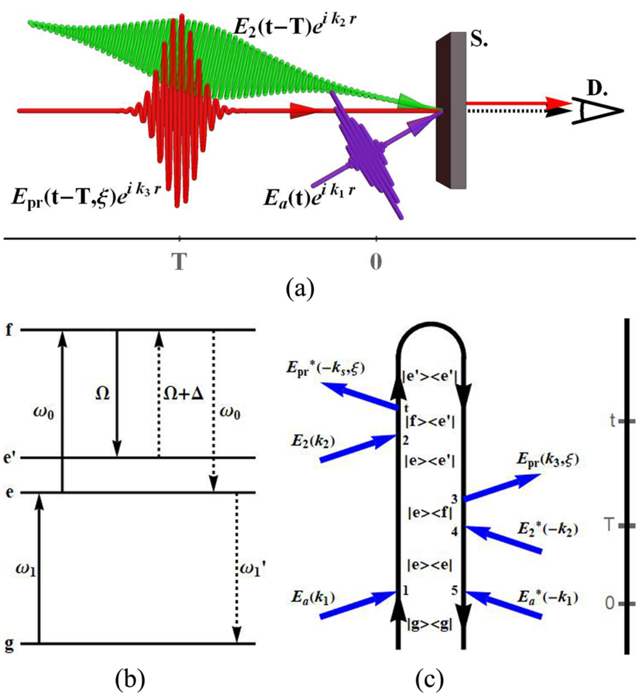

**FIG. 4**. Layout of the SRS signal (a), level scheme (b), and loop diagram (c).

The derivation of the SRS auxiliary signal $\bar{\mathrm{S}}_{SRS}(\Omega,T;\Delta)$ is similar to that of the TA auxiliary signal, but it includes two additional interactions with the field $E_2$. The relevant term in the perturbative expansion of the time-dependent polarization is given by a six-wave mixing quantum amplitude.[12] Its form can be read off from Fig. 4(c) so that the auxiliary signal $\bar{\mathrm{S}}_{SRS}$ is given by the expression

$$\begin{aligned}\bar{\mathrm{S}}_{SRS}&(\Omega,T;\Delta)\\ &= \hbar^5\int_{-\infty}^{\infty}dte^{\mathrm{i}\Omega(t-T)}\int_{-\infty}^{t}d\tau_2E_2(\tau_2)\int_{-\infty}^{\tau_2}d\tau_1E_a(\tau_1)\\ &\quad\cdot\int_{-\infty}^{t}d\tau_3e^{-\mathrm{i}(\Omega+\Delta)(\tau_3-T)}\int_{-\infty}^{\tau_3}d\tau_4E_2^*(\tau_4)\int_{-\infty}^{\tau_4}d\tau_5E_a^*(\tau_5)\\ &\quad\times\langle g|\hat{V}G^\dagger(\tau_4,\tau_5)\hat{V}G^\dagger(\tau_3,\tau_4)\hat{V}^\dagger G^\dagger(t,\tau_3)\\ &\quad\times\hat{V}G(t,\tau_2)\hat{V}^\dagger G(\tau_2,\tau_1)\hat{V}^\dagger|g\rangle.\end{aligned} \tag{27}$$

Equation (21) may be used to calculate the SRS covariance signal generated by stochastic broadband pulse with $\delta$-correlated phases. The off-diagonal SRS covariance spectrum is given by

$$C_{SRS}(\Omega_1,\Omega_2) \propto |\bar{\mathscr{E}}_{pr}|^4\Re\,\bar{\mathrm{S}}_{SRS}(\Omega_1,T;\Omega_2-\Omega_1)\bar{\mathrm{S}}_{SRS}(\Omega_2,T;\Omega_1-\Omega_2). \tag{28}$$

Simulation of the bare and covariance SRS signals is presented in Sec. III A.

### A. Simulation of the stimulated Raman absorption covariance signal

We first simulate the SRS signal for a closed molecular system with three electronic levels $|g\rangle$, $|e\rangle$, and $|f\rangle$, where state $|e\rangle$ has an additional vibrational level $|e'\rangle$; see Fig. 4(b). Equation (27) can be simplified by assuming an impulsive actinic pulse arriving at zero time. A monochromatic field $E_2(t)$ with frequency $\omega_0$ is tuned to be resonant with the $f \to e$ transition, $\omega_0 \sim \omega_{f,e}$. The signal reaches its peak values for frequencies $\Omega$ close to $\omega_0$. Using Eq. (B4) for Green's function of a closed system, we can calculate the resonant contribution to the SRS auxiliary signal,

$$\begin{aligned}\bar{\mathrm{S}}_{SRS}&(\Omega-\omega_0,T;\Delta)\\ &= |\mathscr{E}_a|^2|\mathscr{E}_2|^2\sum_{\nu,\nu',\nu''=e,e'}\frac{\nu^*_{g,\nu''}\nu^*_{\nu'',f}}{\omega_{f,\nu''}-\omega_0-\mathrm{i}\varepsilon}\cdot\frac{\nu_{g,\nu}\nu_{\nu,f}}{\omega_{f,\nu}-\omega_0+\mathrm{i}\varepsilon}\\ &\quad\cdot\frac{|\nu_{\nu',f}|^2e^{\mathrm{i}\Delta T}}{\Omega+\Delta+\omega_{\nu,\nu'}-\mathrm{i}\varepsilon}\left[\frac{1}{\Delta+\omega_{\nu,\nu''}-2\mathrm{i}\varepsilon}-\frac{1}{\omega_{\nu'',\nu'}-\Omega-\mathrm{i}\varepsilon}\right].\end{aligned} \tag{29}$$

Here, $\mathscr{E}_a$ is the actinic pulse amplitude and $\varepsilon$ is the decoherence rate, which is assumed to be equal for all coherent states. The complex coefficients $\nu_{\nu,\nu'}$ are matrix elements of the transition dipole operators $\hat{V}$.

Assuming an impulsive deterministic probe pulse, i.e., $\mathscr{E}_{pr}(\omega,\xi) = \mathscr{E}_{pr}$ and $\xi = 0$, and using Eqs. (29) and (26), we obtain

$$\mathscr{S}_{SRS}(\Omega-\omega_0,T)=2\left|\bar{\mathscr{E}}_{pr}\right|^2\left|\mathscr{E}_a\right|^2\left|\mathscr{E}_2\right|^2\Re\sum_{v,v',v''=e,e'}\frac{v^*_{g,v''}v^*_{v'',f}}{(\omega_{f,v''}-\omega_0)-\mathrm{i}\varepsilon}\cdot\frac{v_{g,v}v_{v,f}}{(\omega_{f,v}-\omega_0)+\mathrm{i}\varepsilon}\cdot\frac{\left|v_{v',f}\right|^2e^{-\mathrm{i}\omega_{v,v''}T-2\varepsilon T}}{\omega_{v'',v'}-\Omega-\mathrm{i}\varepsilon}. \tag{30}$$

The bare SRS signal [Eq. (30)] is plotted in Fig. 5(a) vs $\Omega$ and $T$. The model parameters are given in the caption. It shows an oscillating vertical line at the vibrational frequency $\omega_{e',e}$ = 35 cm$^{-1}$ and the line symmetric with respect to zero. This line corresponds to the quantum path which goes through both electronic $|e\rangle$ and vibrational $|e'\rangle$ levels: the Stokes process $g\to e'\to f\to e\to f\to e\to g$ and the anti-Stokes process $g\to e\to f\to e\to f\to e'\to g$. The oscillation frequency is defined by the same vibrational level spacings, i.e., $\omega_{e',e}$. The signal also contains an oscillating components at frequency $\Omega=\omega_0$, which corresponds to the processes without energy exchange between matter and radiation, such as $g\to e\to f\to e'\to f\to e\to g$. The oscillations with $T$ have the same frequency $\omega_{e',e}$ caused by the Raman transition between $|f\rangle$ and $|e'\rangle$.

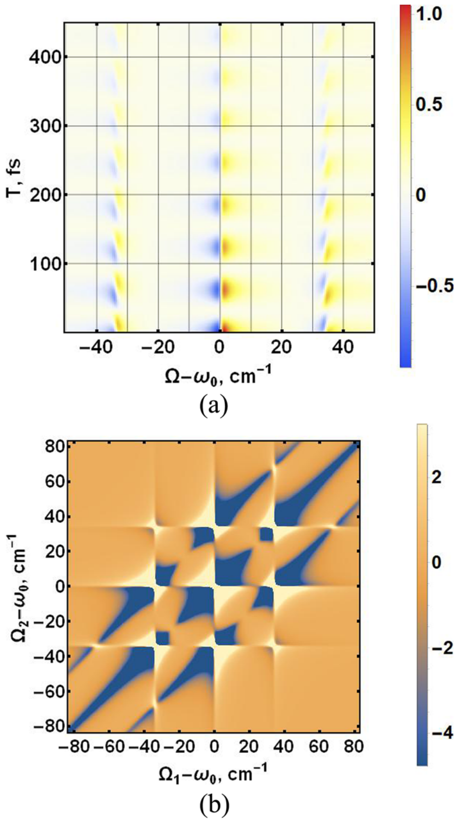

(a)

(b)

**FIG. 5.** (a) SRS signal [Eq. (30)]; (b) SRS covariance signal from the probe pulse with $\delta$-correlated phases [Eq. (28)]. The plots are simulated for a two level model and a single vibrational level; see the level scheme in Fig. 4(b). The model parameters are $\omega_g$ = 770 cm$^{-1}$, $\omega_e$ = 825 cm$^{-1}$, $\omega_{e'}$ = 860 cm$^{-1}$, and $\omega_f$ = 920 cm$^{-1}$; the decoherence rates $\varepsilon$ are equal to 60 ps, $|\mathscr{E}_{pr}|=|\mathscr{E}_a|=1$, and all nonzero transition dipole moments are equal to one.

The 2D SRS covariance signal shown in Fig. 5(b) was calculated by Eq. (28) together with Eq. (29) for the auxiliary signals. We used the level scheme shown in Fig. 4(b) with parameters given in the caption of Fig. 5. The covariance spectrogram has a similar pattern to the TA covariance spectrogram in Fig. 3(b). A detailed comparison of TA spectrogram and SRS shows that their features correspond to different processes. The diagonal lines in the TA spectrum are not identical with horizontal (vertical) lines: the horizontal lines correspond to resonance transitions between valence levels, whereas the diagonal lines represent transitions between vibration levels. In contrast, all three sets of lines (horizontal, vertical, and diagonal) in the SRS correspond to one and the same set of vibrational frequencies. The three-line intersection points also have different interpretation. Each three-line intersection point corresponds to a single symmetric pathway. For instance, the path $g\to e\to f\to e'\to f\to e\to g$ generates a single intersection point (and its symmetric counterpart) in the spectrogram. In Sec. IV, we demonstrate that dynamic information is accessible.

## IV. COVARIANCE SPECTROSCOPY OF A SYSTEM WITH A TIME-DEPENDENT FREQUENCY

### A. The continuous frequency switch model

In previous sections, we demonstrated that statistical processing of the signal generated by the stochastic input allows us to reveal correlations in the flow of nonlinear processes in the media. In this section, we apply nonlinear covariance spectroscopy to study molecular systems with nontrivial dynamics. We assume that the vibrational frequency switches continuously between two values. This models a photoisomerization process, for example. A detailed description of the signal is based on the solution of the Liouville equation for the molecule in a thermal bath. Each molecular orbital weakly interacting with the bath is split into several levels with close energies. This dynamics is described by the stochastic Liouville equation model[31,34] or by the continuous frequency switch (CFS) model formulated in Ref. 10. The excited molecular level dynamics is then described by a time-dependent excitation frequency $\tilde{\omega}(t)$,

$$\tilde{\omega}(t)=\frac{\omega_-+\omega_+}{2}\left[1+\frac{\omega_+-\omega_-}{\omega_++\omega_-}\mathrm{Erf}\left(\frac{t-t_0}{\sigma}\right)\right], \tag{31}$$

where $\mathrm{Erf}(t)=\frac{2}{\sqrt{\pi}}\int_0^t e^{-x^2}dx$. The frequency $\tilde{\omega}(t)$ switches between its value $\omega_-$ at short times, $t\ll t_0$, and $\omega_+$ at large times, $t\gg t_0$; see Fig. 6(a). The slope of the frequency switch is defined by $\sigma$. $e$ is the dynamically evolving excited state, whose quantum evolution results in the Green's function diagonal matrix element $G_{e,e}(t,\tau)$,[12]

$$G_{e,e}(t,\tau)=\frac{-\mathrm{i}}{\hbar}\theta(t-\tau)\exp\left[\mathrm{i}\int_\tau^t d\tau'\tilde{\omega}(\tau')\right], \tag{32}$$

where $\theta(t-\tau)$ is the unit step function. It is useful to represent the Green's function element in the form of the product of two auxiliary functions (the asterisk denotes complex conjugation),

$$G_{e,e}(t,\tau)=\frac{-\mathrm{i}}{\hbar}\theta(t-\tau)\mathscr{K}(t)\mathscr{K}^*(\tau), \tag{33}$$

with

$$\mathscr{K}(t)=\exp\left[\mathrm{i}\int_0^t d\tau\tilde{\omega}(\tau)\right],\qquad \mathscr{K}(0)=1. \tag{34}$$

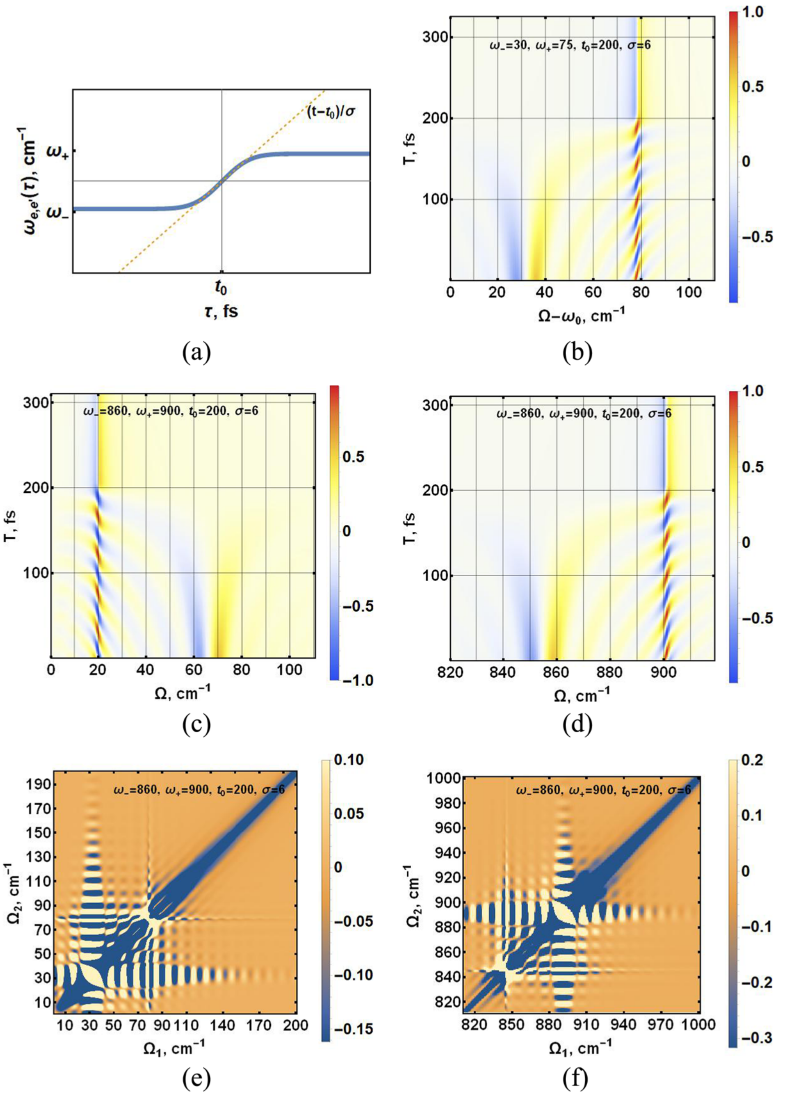

(a) (b) (c) (d) (e) (f)

**FIG. 6**. (a) The time-dependent vibrational frequency in the CFS model [Eq. (31)]; (b) SRS signal calculated by Eq. (42); low-frequency (c) and high-frequency (d) regions of the TA signal [Eq. (38)]; low-frequency (e) and high-frequency (f) TA covariance spectrograms [Eq. (39)]. Parameters of the function Eq. (31) are given inside the panels in inverse centimeters for $\omega_\pm$ and in femtoseconds for $t_0$ and $\sigma$; for other model parameters, see the caption of Fig. 5.

The product $\mathscr{K}(t)\mathscr{K}^*(\tau)$ in Eq. (33) can be understood as an independent time-evolution of the bra and the ket vectors from zero time to some $t$ or $\tau$, respectively. At $t = \tau$, the evolution ends up in the same vector due to the property $\mathscr{K}(t)\mathscr{K}^*(t) \equiv 1$. In Sec. IV B, it will be shown that the observed signal depends on $\tilde{\omega}(t)$ indirectly. It enters the resulting expression through the function $\mathscr{K}(t)$, see Fig. 9. Therefore, the signal can be used to restore the time evolution of $\mathscr{K}(t)$ and consequently of the time evolution of $\tilde{\omega}(t)$. For completeness, the TA covariance signal for the CFS model is given below.

## B. The transient absorption covariance signal of the continuous frequency shift model

We study the TA covariance signal for the model system with three electronic levels $|g\rangle$, $|e\rangle$, and $|f\rangle$, where the energy of a single-excited level $|e\rangle$ switches between two values [we neglect levels $|e'\rangle$ and $|e''\rangle$, see Figs. 2(a) and 2(b)]. The excitation energy trajectory is defined in Eq. (31), $\omega_{e,g}(t) = \tilde{\omega}(t)$. The other electronic levels are static.

To calculate the signal for this dynamical CFS model, it is necessary to recast Eqs. (6) and (7) in terms of temporal integrations. The two contributions to the signals (i) and (ii) can be read off from Figs. 1(b) and 1(c) and now have the forms

$$\bar{S}_{TA(i)}(\Omega, T; \Delta) = 2\hbar^3 \int_{-\infty}^{\infty} dt \int_{-\infty}^{t} d\tau_1 \int_{-\infty}^{t} d\tau_2 e^{i\Omega(t-\tau_2)} e^{-i\Delta(\tau_2 - T)} \times \int_{-\infty}^{\tau_2} d\tau_3 E_a(\tau_1) E_a^*(\tau_3) \langle g|\hat{V} G^\dagger(\tau_2, \tau_3) \times \hat{V}^\dagger G^\dagger(t, \tau_2) \hat{V} G(t, \tau_1) \hat{V}^\dagger |g\rangle, \tag{35}$$

and

$$\bar{S}_{TA(ii)}(\Omega,T;\Delta) = 2\hbar^3\int_{-\infty}^{\infty}dt\int_{-\infty}^{t}d\tau_1\int_{-\infty}^{t}d\tau_2 e^{\mathrm{i}\Omega(t-\tau_2)}e^{-\mathrm{i}\Delta(\tau_2-T)}$$
$$\times\int_{-\infty}^{\tau_2}d\tau_3 E_a(\tau_3)E_a^*(\tau_1)\langle g|\hat{V}G^\dagger(t,\tau_1)$$
$$\times\hat{V}G(t,\tau_2)\hat{V}^\dagger G(\tau_2,\tau_3)\hat{V}^\dagger|g\rangle. \tag{36}$$

Since levels $|g\rangle$, $|e\rangle$, and $|f\rangle$ do not vary with time, the corresponding Green's function diagonal elements coincide with Green's function of free propagation, for instance, $G_{f,f}(t,\tau) = \frac{-\mathrm{i}}{\hbar}\theta(t-\tau)\exp[\mathrm{i}\omega_{f,g}(t-\tau)]$, and the $G_{e,e}(t,\tau)$ matrix element is defined by Eq. (33). Substitution of the actinic field in impulsive approximation allows us to take the integrals over $\tau_3$ and $\tau_1$, so that the final expression for the auxiliary signal $\bar{S}_{TA,dyn}(\Omega,T;\Delta) = \bar{S}_{TA(i)}(\Omega,T;\Delta)+\bar{S}_{TA(ii)}(\Omega,T;\Delta)$ has the form

$$\bar{S}_{TA,dyn}(\Omega,T;\Delta) = -4|\mathscr{E}_a|^2\int_0^{\infty}dt\int_0^t d\tau_2 e^{\mathrm{i}\Omega(t-\tau_2)}e^{-\mathrm{i}\Delta(\tau_2-T)}$$
$$\times\left(|\nu_{e,g}|^2|\nu_{f,e}|^2\cos\left[\int_{\tau_2}^{t}d\tau\tilde{\omega}(\tau)-\omega_{f,g}(t-\tau_2)\right]\right.$$
$$\left.+|\nu_{g,e}|^4\cos\left[\int_{\tau_2}^{t}d\tau\tilde{\omega}(\tau)\right]\right). \tag{37}$$

The bare TA signal is obtained for impulsive deterministic probe pulse, $E_{pr}(t,\xi) = \bar{\mathscr{E}}_{pr}e^{-\mathrm{i}\omega_{pr}T}\delta(t-T)\delta(\xi)$, from Eq. (4) after substitution of Eq. (38). It is

$$\mathscr{S}_{TA,dyn}(\Omega,T) = -8\Im\int_T^{\infty}dte^{\mathrm{i}\Omega(t-T)}\left(|\nu_{e,g}|^2|\nu_{f,e}|^2\cos\left[\int_T^t d\tau\tilde{\omega}(\tau)\right.\right.$$
$$\left.\left.-\omega_{f,g}(t-T)\right]+|\nu_{g,e}|^4\cos\left[\int_T^t d\tau\tilde{\omega}(\tau)\right]\right). \tag{38}$$

To calculate the TA covariance signal generated by stochastic broadband pulse with $\delta$-correlated phases in the CFS model, we have used Eqs. (35) and (36). The off-diagonal TA covariance spectrum is

$$C_{TA,dyn}(\Omega_1,\Omega_2) \propto |\bar{\mathscr{E}}_{pr}|^4\times\Re\,\bar{S}_{TA,dyn}(\Omega_1,T;\Omega_2-\Omega_1)$$
$$\times\bar{S}_{TA,dyn}(\Omega_2,T;\Omega_1-\Omega_2). \tag{39}$$

Equation (38) shows that the TA signal is composed of two parts which show up at two frequency intervals. The low-frequency interval around $\Omega = \omega_- - \omega_{f,g}$ is generated by the first term in Eq. (38) and corresponds to the transition involving the doubly excited state: $g\to e\to f\to e\to g$. The plot calculated by Eq. (38) is shown in panel (c) in Fig. 6. For a static level $e$, i.e., $\omega_-\equiv\omega_+ = 860$ cm$^{-1}$, this part of signal would generate a single nonoscillating line at frequency $\Omega = 60$ cm$^{-1}$ [compare with Fig. 3(a)]. The high-frequency interval [second term in Eq. (38)] located around the frequency $\Omega = \omega_-$, panel (d) in Fig. 6, is generated by the path $g\to e\to g\to e\to g$. The TA covariance spectrum can be also divided into two nonoverlapping regions; see plots in panels (e) and (f) of Fig. 6. TA and SRS covariance signals generated within the CFS model are compared in Sec. IV D.

### C. The stimulated Raman spectroscopy signal for the continuous frequency switch model

To derive the auxiliary SRS signal for the CFS model, we start from Eq. (27) and derive expressions for a three-level system model [Fig. 4(b)], in which the singly excited state has only two vibrational levels $|e\rangle$ and $|e'\rangle$. The level $|e'\rangle$ frequency evolves in time, while other levels $|g\rangle$, $|e\rangle$, and $|f\rangle$ are static. As demonstrated in Sec. IV B, the TA signal may have several contributions at different frequency regimes. The monochromatic component $E_2(t) = \mathscr{E}_2 e^{\mathrm{i}\omega_0 t}$ of the probe field in the SRS protocol [Fig. 4(a)] makes it possible to amplify contribution for a specific quantum pathway by tuning the frequency $\omega_0$. This can be seen from Eq. (29), which describes a closed molecular system, when $\omega_0$ is close to $\omega_{f,e}$ single out $e\to f$ resonances and all other nonresonant terms can be neglected. Therefore, we assume that $\omega_0\simeq\omega_{f,e}$. Among all possible combinations of state-to-state transitions, this choice amplifies the path where after the interaction with the actinic pulse, the system is at the lower-excited state $e$ [Fig. 4(b)] from which it is resonantly excited to the coherent state $|e\rangle\langle f|$ by the monochromatic field $E_2(t)$. The system may be further deexcited by the stochastic probe $E_{pr}$ to the dynamically evolving state $|e'\rangle$ forming the coherence $|e'\rangle\langle e|$ between the vibrational levels. The dynamics is assumed to be slow in comparison with other fast optical processes so that the system can be described by the CFS model with $\omega_{e',e} = \tilde{\omega}(t)$ so that the nontrivial time evolution of $|e'\rangle$ is described by Eq. (33), the states $|g\rangle$, $|e\rangle$, and $|f\rangle$ are static, and their evolution is described by free propagation Green's function. The time-dependence of $\tilde{\omega}(t)$ is approximated by Eq. (31); see Fig. 6(a). Assuming an impulsive actinic pulse and a monochromatic $E_2$ [Eq. (27)], we obtain for the auxiliary signal

$$\bar{S}_{SRS,dyn}(\Omega-\omega_0,T;\Delta)$$
$$= \hbar|\mathscr{E}_a|^2|\mathscr{E}_2|^2\frac{|\nu_{e,g}|^2|\nu_{e,f}|^2|\nu_{e',f}|^2}{(\omega_{f,e}-\omega_0)^2+\varepsilon^2}e^{\mathrm{i}\Delta T}\int_0^{\infty}dt\mathscr{K}^*(t)e^{\mathrm{i}\Omega t-\varepsilon t}$$
$$\times\int_0^t d\tau\mathscr{K}(\tau)e^{-\mathrm{i}(\Omega+\Delta)\tau-\varepsilon\tau}, \tag{40}$$

where the function $\mathscr{K}(t)$ describes the nontrivial phase evolution due to the internal dynamics of the system [Eq. (34)]. Note that the auxiliary signal $\bar{S}_{SRS,dyn}(\Omega-\omega_0,T;\Delta)$ contains also a term which corresponds to the sequence of quantum transitions through the static states only,

$$\hbar|\mathscr{E}_a|^2|\mathscr{E}_2|^2\frac{|\nu_{e,g}|^2|\nu_{e,f}|^2|\nu_{e,f}|^2}{(\omega_{f,e}-\omega_0)^2+\varepsilon^2}\frac{e^{\mathrm{i}\Delta T}}{(\Omega+\mathrm{i}\varepsilon)(\Delta-2\mathrm{i}\varepsilon)}. \tag{41}$$

Contributions from such types of terms to the SRS covariance signal were studied in Sec. III, and they will be omitted in our further consideration. For impulsive, deterministic probe pulse, $E_{pr}(t,\xi) = \mathscr{E}_{pr}e^{-\mathrm{i}\omega_p T}\delta(t-T)\delta(\xi)$. The SRS signal is

$$\mathscr{S}_{SRS}(\Omega,T) = 2|\mathscr{E}_{pr}|^2|\mathscr{E}_a|^2|\mathscr{E}_2|^2\frac{|\nu_{e,g}|^2|\nu_{e,f}|^2|\nu_{e',f}|^2}{(\omega_{f,e}-\omega_0)^2+\varepsilon^2}$$
$$\times\Im\,\mathscr{K}(T)\int_T^{\infty}dte^{\mathrm{i}\Omega(t-T)-\varepsilon(t-T)}\mathscr{K}^*(t). \tag{42}$$

It is instructive to compare the bare SRS signal displayed vs $\Omega$ and $T$ in panel (b) with the TA signal shown in panels (c) and (d) of Fig. 6. Note that the TA signal was calculated for a three-level system with changing single-excited level $|e\rangle$, while the SRS signal is plotted for the system with an additional time-dependent vibrational level $|e'\rangle$. Nevertheless, both signals show identical reflection, total phase, and position on the frequency axis patterns. We shall consider the SRS signal in panel (b) of Fig. 6 separately. For long-$T$, the pattern reduces to a single nonoscillating line parallel to the $T$ axis at $\Omega = \omega_+$ and coincides with the pattern which would be generated in the static case. The asymptotic regime can be seen from Eq. (42) for $T \gg t_0$, when $\mathscr{K}(t \gg t_0) \propto e^{i\omega_+ t}$. The initial frequency $\omega_-$ reveals itself at $T \sim 0$ as the smallest value of $\Omega$ where the signal crosses zero. In this limit, the resonant contribution $\Im \frac{1}{i(\Omega-\omega_-)-\epsilon}$ can be extracted from the integral in Eq. (42).

The issue of simultaneous temporal and spectral resolution in the SRS signal has been discussed in Ref. 11. The signal depends on the entire trajectory $\tilde{\omega}(t)$ between the stimulation time $T$ and the detection time $t$ and is not related directly to the single snapshot $\tilde{\omega}(T)$; see Eq. (42). In the static case, it would be enough to calculate Fourier transform over $T$ for a given $\Omega$ to find the oscillation frequency, which is the interval between the vibrational levels $\omega_{e',e}$; see discussion in Sec. II C. In the dynamical case, any integration over $T$ mixes values of $\tilde{\omega}(t)$ at different times and cannot be interpreted in a simple manner. From Eq. (42), one can see that the quantity, which can be formally extracted from the signal, is $\tilde{\mathscr{K}}(\Omega)$, which is Fourier transform of $\mathscr{K}(t)$ and $\mathscr{S}_{SRS}(\Omega, T = 0) \propto \tilde{\mathscr{K}}(\Omega)$; see Fig. 7. $\mathscr{S}_{SRS}(\Omega, T = 0)$ represents a special limit $\lim_{T\to 0} \mathscr{S}_{SRS}(\Omega, T)$ and, thus, is not directly achievable in experiment. Calculation of the Fourier transform at any nonzero $T$ gives a quantity with a reduced amount of information about $\tilde{\omega}(t)$. The latter problem can be partially avoided by using chirped pulses. A similar plot: signal $\mathscr{S}_{SRS}$ vs $\Omega$ and $T'$, where $T'$ is effective time of chirped pulse arrival, can be generated. Fourier transform over $\Omega$ with a given $T'$ now gives the quantity $\int_0^\infty dt w(t, T') e^{i\Omega(t-T)-\epsilon(t-T)} \mathscr{K}^*(t)$ with some weight function $w(t)$. Covariance spectroscopy, as demonstrated in Sec. IV D, is a tool which allows us to extract unmodified function $\tilde{\mathscr{K}}(\Omega)$.

### D. Continuous frequency shift dynamical parameters revealed from the stimulated Raman spectroscopy covariance spectrum

The covariance of the SRS signal obtained for $\delta$-correlated phases is calculated by

$$C_{SRS}(\Omega_1, \Omega_2) \propto \Re \bar{S}_{SRS}(\Omega_1 + \omega_0, 0; \Omega_2 - \Omega_1) \times \bar{S}_{SRS}(\Omega_2 + \omega_0, 0; \Omega_1 - \Omega_2), \tag{43}$$

where $\bar{S}_{SRS}(\Omega, T; \Delta)$ is the auxiliary frequency-dispersed SRS signal. The SRS covariance spectrum for the case of static excitation frequencies derived in Sec. III consists of diagonal and horizontal lines without any marks of interference patterns. Typical SRS covariance spectra of a three-level system ($|g\rangle$, $|e\rangle$, and $|f\rangle$) and dynamically changing vibrational level $|e'\rangle$ are plotted in Fig. 7 for various parameters of the CFS model. The covariance spectra contain interference patterns, and variation of dynamical

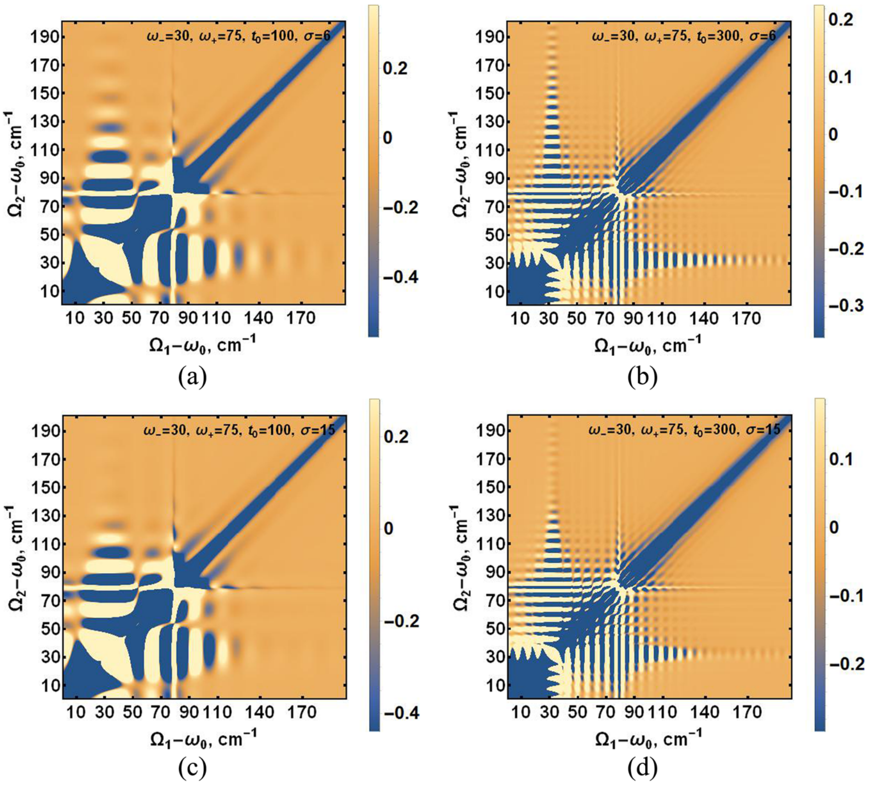

(a) (b)

(c) (d)

**FIG. 7**. SRS covariance signals [Eqs. (43) and (40)] of the CFS model with [(a) and (b)] sharp, $\sigma$ = 6 fs, and [(c) and (d)] slow, $\sigma$ = 15 fs, slopes probed by stochastic pulse with $\delta$-correlated phases plotted vs $t_0$ = 100 fs and 300 fs. Other parameters are taken to be the same for each plot: $\omega_{e,g}$ = 800 cm$^{-1}$, $\omega_-$ = 30 cm$^{-1}$, $\omega_+$ = 75 cm$^{-1}$, and decoherence time 60 ps.

parameters leads to a continuous change in the pattern. In particular, the larger the $t_0$, the more the oscillatory cycles we observe, while the pattern is less sensitive to the frequency switch rate governing by $\sigma$. In addition to the qualitative observation of dynamical changes, quantitative information about the internal dynamics of the system can be also extracted from SRS covariance spectra, through asymptotic analysis of the covariance (43) at large values of frequencies $\Omega_1$ and $\Omega_2$.

The SRS covariance spectra are shown in Fig. 7. Note that $T$ is a dummy parameter in the covariance spectrum. Considering the asymptotic of $\bar{S}(\Omega_1+\omega_0,0;\Omega_2-\Omega_1)$ [Eq. (40)] at $\Omega_1 \gg \tilde{\omega}_+$ ($\omega_+$ is the maximum characteristic frequency of $\omega_{e',e}$), the $\tau$ dependence of the second integral in (42) can be simplified. The large-$\Omega_1$ asymptotic, up to an $\Omega$-independent prefactor, is

$$\bar{S}_{SRS}(\Omega_1+\omega_0,0;\Omega_2-\Omega_1) \simeq -\frac{\mathcal{K}^*(0)}{i\Omega_1-\varepsilon}\int_0^\infty dt\mathcal{K}(t)e^{i(\Omega_1-\Omega_2)t-2\varepsilon t}. \tag{44}$$

In the same large-$\Omega_1$ limit, the auxiliary signal with interchanged arguments reduces to

$$\bar{S}_{SRS}(\Omega_2+\omega_0,0;\Omega_1-\Omega_2) \simeq \frac{\mathcal{K}(0)}{i\Omega_1+\varepsilon}\int_0^\infty dt\mathcal{K}^*(t)e^{i\Omega_2 t-\varepsilon t} \times\left(1-e^{-i\Omega_1 t-\varepsilon t}\right). \tag{45}$$

The traces of the above asymptotics are clearly seen in the $\Re\bar{S}_{SRS}(\Omega_1+\omega_0,0;\Omega_2-\Omega_1)$ vs $\Omega_1$ and $\Omega_2$ plot in Fig. 8(a). In particular, it follows from Eq. (44) that $\bar{S}_{SRS}(\Omega_1+\omega_0,0;\Omega_2-\Omega_1)$ is almost a constant along each line from the family of lines: $\Omega_2 = \Omega_1 - \tilde{\Omega}$, when $\tilde{\Omega} \gg \omega_+$. The real and the imaginary part profiles of $\bar{S}_{SRS}(\Omega_1+\omega_0,0;\Omega_2-\Omega_1)$ calculated along a diagonal line are shown in the panel (b) in Fig. 8. Note that the imaginary part nullifies, while the real part is a nonzero constant solely depending on $\tilde{\Omega}$. The Fourier transform of $\mathcal{K}(t)$ is contained in the large-$\Omega_1$ asymptotic of the auxiliary signal with inverse arguments [Eq. (45)]. Asymptotic expression for the covariance at large $\Omega_1$ is

$$C_{SRS}(\Omega_1,\Omega_2) \simeq \frac{1}{\Omega_1^2+\varepsilon^2}\Re\big(\tilde{\mathcal{K}}(\Omega_2)-\tilde{\mathcal{K}}(\Omega_2-\Omega_1)\big)\tilde{\mathcal{K}}^*(\Omega_2-\Omega_1), \tag{46}$$

$$\tilde{\mathcal{K}}(\Omega) = \int_0^\infty d\tau\mathcal{K}(\tau)e^{i\Omega\tau-\varepsilon\tau}.$$

The covariance calculated along the line $\Omega_1 = \Omega_2 + \tilde{\Omega}$ is therefore proportional to $\frac{1}{(\Omega_1-\tilde{\Omega})^2+\varepsilon^2}\Re\tilde{\mathcal{K}}(\Omega_1-\tilde{\Omega})\tilde{\mathcal{K}}^*(-\tilde{\Omega})$, from which the quantity $\tilde{\mathcal{K}}(\Omega)$ can be directly extracted by small variations of $\Omega_1$ around the large value $\tilde{\Omega}$.

The covariance profile along the diagonal line in panel (c) is compared in Fig. 8(d) with the Fourier transform of the original function $\mathcal{K}(t)$ [see Fig. 9(d)]. Based on the good agreement between two curves, we conclude that the dynamical information about the system in the CFS model can be extracted from the SRS covariance signal.

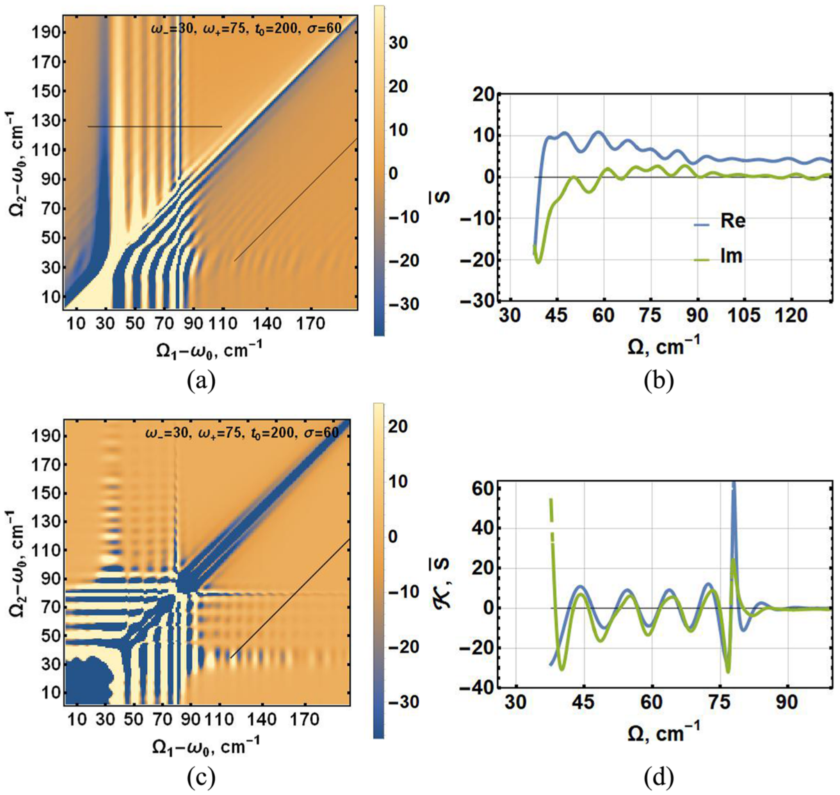

(a)

(b)

(c)

(d)

**FIG. 8**. (a) 2D density plot of the auxiliary signal $\bar{S}_{SRS}(\Omega_1,0;\Omega_2-\Omega_1)$ in variables $\Omega_1$ and $\Omega_2$; (b) real and imaginary parts of $\bar{S}_{SRS}(\Omega_1,0;\Omega_2-\Omega_1)$ calculated along the solid diagonal line in plot (a); (c) SRS covariance signal for the CFS model; (d) SRS signal (green) calculated along the black thin line shown in plot (c) compared with the Fourier transform of $\mathcal{K}(t)$ (blue).

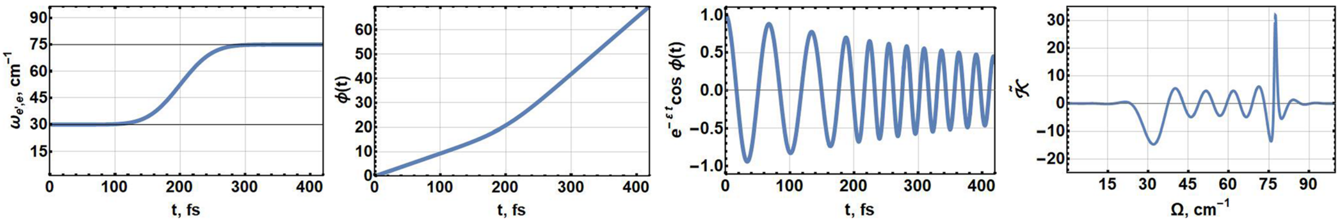

(a) (b) (c) (d)

**FIG. 9**. (a) Time-dependent vibrational frequency in the CFS model [Eq. (31)] calculated for $\omega_- = 30$ cm$^{-1}$, $\omega_+ = 75$ cm$^{-1}$, and $\sigma = 55$ fs; (b) and (c) $\mathcal{K}(t) = e^{-i\phi(t)}$, $\phi(t) = \int_0^t \omega_{e',e}(\tau)d\tau$; (d) Fourier transform of $\mathcal{K}(t)$.

In summary, we note that the method used to obtain $\tilde{\mathcal{K}}(\Omega)$ can be extended in various ways. To improve the quality, one can choose several different cross sections in the plane $(\Omega_1, \Omega_2)$ using the asymptotic expression (46) and perform statistical averaging of the obtained data. We have considered the covariance of the signal with itself. However, the covariance can be calculated with another SRS signal, whose properties are known a priori. Such heterodyne SRS covariance signal will allow to relax the requirements for asymptotic values of $\Omega$. Finally, we note that the SRS covariance signal has an advantage with respect to the TA covariance signal analyzed in Sec. IV B. The time-reversal symmetry of SRS process simplifies the resulting expressions for the covariance spectrum [compare Eqs. (37) and (27)] and allows us to make the asymptotic analysis.

## V. CONCLUSIONS

We analyzed the mean and the covariance signals generated by transmitted broadband probe pulse modulated by frequency-dependent stochastic phase. We have demonstrated how stochastic light may be used to improve the temporal and spectral resolutions of nonlinear signals. The probe beam interferes with the radiation generated by the sample polarized by the same probe pulse. The detected electric field intensity is proportional to the product of probe pulse envelope and to the time-dispersed auxiliary signal $\bar{S}(t, T; \tau)$ [or frequency-dispersed $\bar{S}(\Omega, T; \Delta)$] dressed by the same probe pulse field.[12] In measurements involving deterministic light, the frequency-gated signal provides only integrated spectral information at instant of time $T$ [in impulsive approximation for the probe field $\mathcal{S}(\Omega, T) = 2|\mathcal{E}_{pr}|^2\Im \int_{-\infty}^{\infty}\frac{d\Delta}{2\pi}\bar{S}(\Omega, T; \Delta)$]. We showed that the probe pulse coherence breaking allows us to disentangle the time interval and spectral range covered by the probe pulse [Eqs. (13) and (14)]. Covariance spectroscopy involves averaging the signals generated by interaction of the sample with random chirped pulses. The governing control parameter is the frequency correlation range, $1/\mathcal{T}_C$. We considered two types of covariance signals, TA and SRS, generated by an actinic pulse and broadband probe pulse with a stochastic phase. The covariance spectra were calculated for the broadband probe pulses modulated by a stochastic phase $\xi(\omega)$. Control of the two- and four-point correlation functions allows us to amplify certain components of the signal. The main theoretical results are Eqs. (8) and (11) for the 2D covariance spectrum.

For a closed molecular system and $\delta$-correlated phases $(\langle\xi(\Omega)\xi(\Omega + \Delta)\rangle_\xi = \delta(\Delta))$, the 2D covariance spectra of TA and SRS signals represent a set of vertical, horizontal, and diagonal linear features. The characteristic frequencies of these lines reveal the molecular transition frequencies. For a closed system (with static frequencies), covariance spectroscopy carries the same amount of information as the TA and SRS signals generated by deterministic light. For a deterministic probe, the data analysis is based on Fourier transform with respect to the probe pulse arrival time $T$.[9,35] Both approaches, however, require repeated measurements either to perform statistical averaging or to calculate the Fourier transform with a required accuracy.

In experiments focusing on ultrafast molecular dynamics, tracking the nuclear wave packet dynamics in various regions of the excited-state potential energy surface is of interest. In frames of CFS model, we demonstrated that the covariance spectroscopy allows us to reveal the time-flow of the molecular system dynamics. We developed an analytic approach for SRS covariance spectrum analysis that restores the function $\tilde{\mathcal{K}}(\Omega)$ [Eqs. (34) and (46)] of quantum evolution defined in frequency domain and gave arguments that this quantity *cannot be extracted from the bare TA and SRS signals.*

Therefore, in the case of static energy levels (closed molecular system), stochastic spectroscopy can be used to resolve the vibrational levels,[6–8] while it gives a principally new tool for study of open molecular system with time-dependent vibrational frequencies. Further improvement of the method can be done with a "heterodyne" covariance spectrum, i.e., covariance of a signals generated by interaction of stochastic pulse with the sample and with a reference material. Another type of modifications is various choices of the two- and the four-point phase correlation functions. In this paper, we have discussed the simplest case of $\delta$-correlated phases.

## ACKNOWLEDGMENTS

The authors acknowledge the National Science Foundation (Grant No. CHE-1663822) and the support of the Chemical Sciences, Geosciences, and Biosciences Division, Office of Basic Energy Sciences, Office of Science, U.S. Department of Energy, through Award Nos. DE-FG02-04ER15571 (for S.A.) and DE-SC0019484 (for V.A.O.). The authors thank Daeheum Cho and Adam Brunauer for useful discussions.

## APPENDIX A: THE BROWNIAN PHASE MODEL

The one-dimensional Brownian motion (Wiener random process) is a mathematical model for description of phase $\xi(\omega)$ as a random continuous function of $\omega$.[36] We represent the phase increment in a form of integral of a white noise, $\xi(\Delta) - \xi(0) = \int_0^\Delta dW_\xi$. The probability density function of the increment follows normal distribution with zero mean value, which variance grows linearly with respect to the interval length, $\langle[\xi(\Delta) - \xi(0)]^2\rangle_\xi = \mathscr{T}_C\Delta$, where $\mathscr{T}_C$ is the effective range of phase correlation. The Gaussian nature of increments permits the calculation of the autocorrelation functions,

$$\langle e^{i\xi(\Omega)-i\xi(\Omega-\Delta)}\rangle_\xi = \frac{1}{\sqrt{4\pi\mathscr{T}_C|\Delta|}}\int dx e^{ix-x^2/(4\mathscr{T}_C|\Delta|)} = e^{-|\Delta|\mathscr{T}_C}. \tag{A1}$$

The autocorrelation function of a combination of increments can be calculated similarly taking into account that all increments, which correspond to nonintersecting intervals, are distributed independently. The average value of four phases is a piecewise defined function of four arguments,

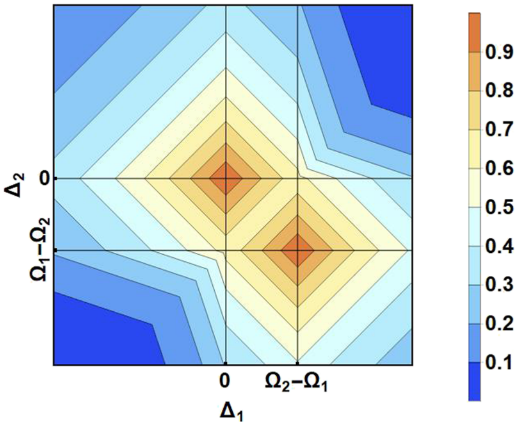

**FIG. 10**. Schematic plot of $\Xi(\Omega_1, \Omega_2, \Delta_1, \Delta_2)$ [Eq. (A2)] as a function of $\Delta_1$ and $\Delta_2$ with fixed $\Omega_2 > \Omega_1$ for the Brownian phase model. The function has two maxima and decays exponentially.

$$\Xi(\Omega_1,\Omega_2,\Delta_1,\Delta_2) \equiv \langle e^{i\xi(\Omega_1+\Delta_1)-i\xi(\Omega_1)+i\xi(\Omega_2+\Delta_2)-i\xi(\Omega_2)}\rangle_\xi = \begin{cases} e^{-(|\Delta_1|+|\Delta_2|)\mathscr{T}_C}, & |\Delta_1| + |\Delta_2| \le |2\Omega_2 - 2\Omega_1 + \Delta_2 - \Delta_1|; \\ e^{|2\Omega_2-2\Omega_1+\Delta_2-\Delta_1|\mathscr{T}_C-2(|\Delta_1|+|\Delta_2|)\mathscr{T}_C}, & |\Delta_2 - \Delta_1| \le |2\Omega_2 - 2\Omega_1 + \Delta_2 - \Delta_1|; \\ e^{-|2\Omega_2-2\Omega_1+\Delta_2-\Delta_1|\mathscr{T}_C}, & |\Delta_2 + \Delta_1| \le |2\Omega_2 - 2\Omega_1 + \Delta_2 - \Delta_1|; \\ e^{-(|\Delta_1|-|\Delta_2|)\mathscr{T}_C}, & \Delta_1 + \Delta_2 \ge |2\Omega_2 - 2\Omega_1 + \Delta_2 - \Delta_1|, \quad \Delta_2 \le 0; \\ e^{-(|\Delta_2|-|\Delta_1|)\mathscr{T}_C}, & \Delta_1 + \Delta_2 \le |2\Omega_2 - 2\Omega_1 + \Delta_2 - \Delta_1|, \quad \Delta_1 \ge 0; \\ e^{-(3|\Delta_1|+|\Delta_2|)\mathscr{T}_C}, & \Delta_1 - \Delta_2 \ge |2\Omega_2 - 2\Omega_1 + \Delta_2 - \Delta_1|, \quad \Delta_1 \le 0; \\ e^{-(3|\Delta_2|+|\Delta_1|)\mathscr{T}_C}, & \Delta_1 - \Delta_2 \ge |2\Omega_2 - 2\Omega_1 + \Delta_2 - \Delta_1|, \quad \Delta_2 \ge 0. \end{cases} \tag{A2}$$

In the text, we also use another combination of phases, which average value is connected with function $\Xi$ as follows: $\langle e^{i\xi(\Omega_1+\Delta_1)-i\xi(\Omega_1)-i\xi(\Omega_2+\Delta_2)+i\xi(\Omega_2)}\rangle_\xi = \Xi(\Omega_1, \Omega_2 + \Delta_2, \Delta_1, -\Delta_2)$.

## APPENDIX B: THE TRANSIENT ABSORPTION SIGNAL

In this section, we derive expression for the deterministic TA signal.[9,12,22,25] The signals is defined as the change of total photon number, $\int \frac{d}{dt}\langle\hat{E}^\dagger(t)\hat{E}(t)\rangle dt$. The Heisenberg equation of motion for the field operator, $\frac{d}{dt}\hat{E} = \frac{i}{\hbar}[H, \hat{E}] + \left(\frac{\partial}{\partial t}\hat{E}\right)_H$, allows us to represent the signal in the form

$$S = 2\Im\int_{-\infty}^{\infty} dt \,\mathrm{Tr}\left[\hat{E}^\dagger(t)\hat{V}(t)\rho(t)\right]. \tag{B1}$$

The density operator $\rho(t)$ is defined in the joint field-matter space of the entire system, and $\Im$ stands for the imaginary part. For the classical optical pulse, the electric field operator is replaced by its expectation value $\langle\hat{E}(t)\rangle = E(t)$. The sample is prepared in a superposition state at zero time, which is modeled by interaction with an actinic pulse, $E_a(t)$. The probe pulse arrives after the time delay $T$; see Eq. (3). The frequency-dispersed signal is expressed in terms of positive frequency polarization $\mathscr{P}(t)$,

$$S(\Omega) = \frac{2}{\hbar}\Im\,\mathscr{E}^*_{pr}(\Omega)\int_{-\infty}^{\infty} dt\mathscr{P}(t)e^{i\Omega(t-T)}, \tag{B2}$$

where $\mathscr{P}(t) = \hbar\mathrm{Tr}\left[\hat{V}(t)\rho(t)\right]$. Evolution of the matter density matrix, $\rho(t)$, is governed by the Liouville equation, $\hbar\dot{\rho}(t) = -i[H, \rho]$. Its solution yields

$$\mathscr{P}(t) = \hbar\mathrm{Tr}\left[\hat{V}(t)\ \mathrm{Texp}\left(-\frac{i}{\hbar}\int_{-\infty}^{t} d\tau[H_{int}(\tau), \cdot]\right)\rho_0\right]. \tag{B3}$$

Specific signals are obtained by expanding Eq. (B3) to the desired order in $H_{int}$. The TA signal is defined as the change in the probe intensity and must contain two interactions with the actinic field. Therefore, the signal is the third-order expansion of the exponent in Eq. (B3). The expansion contains two contributions, see loop diagrams in Fig. 1(b), which originate from the third-order expansion of the bra and ket vectors in the quantum expectation value $\langle\Psi(t)|\hat{V}(t)|\Psi(t)\rangle$. By the convention,[33] the time-evolution along the loop goes from the ket to the bra, and the last in time interaction occurs on the ket side. For a time independent Hamiltonian, the retarded Green's function of free propagation depends on the time interval. In the frequency domain, it is

$$\tilde{G}(\omega) = -\frac{1}{\hbar}\frac{\mathrm{i}}{\omega - (H_0/\hbar - \omega_g) + \mathrm{i}\varepsilon}, \tag{B4}$$

where $\hbar\omega_g$ is the ground state energy. Each diagram contributes to the TA signal. In Fig. 1 (i), the actinic pulse $\mathscr{E}_a(\omega_1)$ electronically excites the molecule to the level $|\nu\rangle$. Then, the molecule propagates until de-exciting to the level $|\nu'\rangle$ by the probe pulse $\bar{\mathscr{E}}_{pr}(\Omega)$ at the frequency $\Omega$. The ket vector propagates backward in time. After excitation by the $\mathscr{E}_a^*(\omega_1')$ pulse to the level $\langle\mu|$, it propagates until stimulated emission by the probe pulse $\bar{\mathscr{E}}_{pr}^*(\Omega+\Delta)$ to the level $\langle\nu'|$. The system propagates further with the energy $\omega_1' - \Omega - \Delta$. Similarly, one reads diagram (ii). The contributions to the auxiliary signal $\bar{S}_{TA}$ are given by Eqs. (6) and (7). They can be further simplified for an impulsive actinic pulse, $E_a(t) = \mathscr{E}_a\delta(t)$,

$$\begin{aligned}\langle V\tilde{G}^\dagger(\omega_1)V^\dagger\tilde{G}^\dagger(\omega_2)V\tilde{G}(\omega_3)V^\dagger\rangle = \frac{\mathrm{i}^2(-\mathrm{i})}{\hbar^3}\sum_{\nu,\nu',\mu} \nu_{g,\nu}\nu^*_{\nu,\nu'}\nu_{\nu',\mu}\nu^*_{\mu,g}\\ \times\frac{1}{\omega_1-\omega_{\nu,g}-\mathrm{i}\varepsilon_\nu}\frac{1}{\omega_2-\omega_{\nu',g}-\mathrm{i}\varepsilon_{\nu'}}\\ \times\frac{1}{\omega_3-\omega_{\mu,g}+\mathrm{i}\varepsilon_\mu},\end{aligned} \tag{B5}$$

$$\begin{aligned}\langle V\tilde{G}^\dagger(\omega_1)V\tilde{G}(\omega_2)V^\dagger\tilde{G}(\omega_3)V^\dagger\rangle = \frac{\mathrm{i}(-\mathrm{i})^2}{\hbar^3}\sum_{\nu,\nu',\mu} \nu_{g,\nu}\nu_{\nu,\nu'}\nu^*_{\nu',\nu''}\nu^*_{\mu,g}\\ \times\frac{1}{\omega_1-\omega_{\nu,g}-\mathrm{i}\varepsilon_\nu}\frac{1}{\omega_2-\omega_{\nu',g}+\mathrm{i}\varepsilon_{\nu'}}\\ \times\frac{1}{\omega_3-\omega_{\mu,g}+\mathrm{i}\varepsilon_\mu}.\end{aligned} \tag{B6}$$

Substitution of $E_a(t) = \mathscr{E}_a\delta(t)$ into Eqs. (6) and (7) and integration over $\omega_1$ and $\omega_1'$ yield Eqs. (22) and (23).

## REFERENCES

[1] S. Asaka, H. Nakatsuka, M. Fujiwara, and M. Matsuoka, "Accumulated photon echoes with incoherent light in $Nd^{3+}$-doped silicate glass," Phys. Rev. A **29**, 2286–2289 (1984).

[2] R. Beach and S. R. Hartmann, "Incoherent photon echoes," Phys. Rev. Lett. **53**, 663–666 (1984).

[3] T. Kobayashi, A. Terasaki, T. Hattori, and K. Kurokawa, "The application of incoherent light for the study of femtosecond-picosecond relaxation in condensed phase," Appl. Phys. B **47**(2), 107–125 (1988).

[4] N. Morita and T. Yajima, "Ultrahigh-time-resolution coherent transient spectroscopy with incoherent light," Phys. Rev. A **30**, 2525–2536 (1984).

[5] J. L. Hall, M. Notcutt, and J. Ye, "Improving laser coherence," in *Laser Spectroscopy: Proceedings of the XVII International Conference, Aviemore, Scotland, UK, 19-24 2005* (World Scientific, 2005), pp. 3–13.

[6] V. Kimberg and N. Rohringer, "Stochastic stimulated electronic x-ray Raman spectroscopy," Struct. Dyn. **3**(3), 034101 (2016).

[7] C. Weninger, M. Purvis, D. Ryan, R. A. London, J. D. Bozek, C. Bostedt, A. Graf, G. Brown, J. J. Rocca, and N. Rohringer, "Stimulated electronic x-ray Raman scattering," Phys. Rev. Lett. **111**, 233902 (2013).

[8] C. Weninger and N. Rohringer, "Stimulated resonant x-ray Raman scattering with incoherent radiation," Phys. Rev. A **88**, 053421 (2013).

[9] S. Mukamel, *Principles of Nonlinear Optical Spectroscopy* (Oxford University Press, 1995).

[10] K. E. Dorfman, B. P. Fingerhut, and S. Mukamel, "Broadband infrared and Raman probes of excited-state vibrational molecular dynamics: Simulation protocols based on loop diagrams," Phys. Chem. Chem. Phys. **15**, 12348 (2013).

[11] S. Mukamel and J. D. Biggs, "Communication: Comment on the effective temporal and spectral resolution of impulsive stimulated Raman signals," J. Chem. Phys. **134**(16), 161101 (2011).

[12] M. Kowalewski, B. P. Fingerhut, K. E. Dorfman, K. Bennett, and S. Mukamel, "Simulating coherent multidimensional spectroscopy of nonadiabatic molecular processes: From the infrared to the x-ray regime," Chem. Rev. **117**(19), 12165–12226 (2017).

[13] N. Christensson, Y. Avlasevich, A. Yartsev, K. Müllen, T. Pascher, and T. Pullerits, "Weakly chirped pulses in frequency resolved coherent spectroscopy," J. Chem. Phys. **132**(17), 174508 (2010).

[14] D. Fu, G. Holtom, C. Freudiger, X. Zhang, and X. S. Xie, "Hyperspectral imaging with stimulated Raman scattering by chirped femtosecond lasers," Phys. Chem. B **117**, 4634 (2013).

[15] I. A. Shkrob, D. A. Oulianov, R. A. Crowell, and S. Pommeret, "Frequency-domain 'single-shot' ultrafast transient absorption spectroscopy using chirped laser pulses," J. Appl. Phys. **96**(1), 25–33 (2004).

[16] D. Polli, D. Brida, S. Mukamel, G. Lanzani, and G. Cerullo, "Effective temporal resolution in pump-probe spectroscopy with strongly chirped pulses," Phys. Rev. A **82**, 053809 (2010).

[17] R. Loudon, *The Quantum Theory of Light* (Oxford University Press, 2000).

[18] D. B. Turner, P. C. Arpin, S. D. McClure, D. J. Ulness, and G. D. Scholes, "Coherent multidimensional optical spectra measured using incoherent light," Nat. Commun. **4**, 2298 (2013).

[19] E. Saldin, E. Schneidmiller, and M. Yurkov, *The Physics of Free Electron Laser* (Springer-Verlag, Berlin, 2000).

[20] J. N. Galayda, J. Arthur, D. F. Ratner, and W. E. White, "X-ray free-electron lasers—Present and future capabilities," J. Opt. Soc. Am. B **27**(11), B106–B118 (2010).

[21] C. Bressler and M. Chergui, "Molecular structural dynamics probed by ultrafast x-ray absorption spectroscopy," Annu. Rev. Phys. Chem. **61**(1), 263–282 (2010).

[22] J. Che, W. Zhang, and Y. Yan, "A classical time-frequency theory of transient absorption spectroscopy," J. Chem. Phys. **106**(17), 6947–6956 (1997).

[23] L. X. Chen and X. Zhang, "Photochemical processes revealed by x-ray transient absorption spectroscopy," J. Phys. Chem. Lett. **4**(22), 4000–4013 (2013).

[24] R. Berera, R. van Grondelle, and J. T. M. Kennis, "Ultrafast transient absorption spectroscopy: Principles and application to photosynthetic systems," Photosynth. Res. **101**, 105–108 (2009).

[25] R. Santra, V. S. Yakovlev, T. Pfeifer, and Z.-H. Loh, "Theory of attosecond transient absorption spectroscopy of strong-field-generated ions," Phys. Rev. A **83**, 033405 (2011).

[26] M. Badieirostami, A. Adibi, H.-M. Zhou, and S.-N. Chow, "Model for efficient simulation of spatially incoherent light using the wiener chaos expansion method," Opt. Lett. **32**(21), 3188–3190 (2007).

[27] R. Eramo, P. C. Pastor, and S. Cavalieri, "Analytic random-walk model for the coherence of a frequency comb," Phys. Rev. A **97**, 033842 (2018).

[28] R. Feced and M. N. Zervas, "Effects of random phase and amplitude errors in optical fiber bragg gratings," J. Lightwave Technol. **18**(1), 90 (2000).

[29] C. W. Freudiger, W. Min, B. G. Saar, S. Lu, G. R. Holtom, C. He, J. C. Tsai, J. X. Kang, and X. S. Xie, "Label-free biomedical imaging with high sensitivity by stimulated Raman scattering microscopy," Science **322**, 1857 (2008).

[30] G. Fumero, G. Batignani, K. E. Dorfman, S. Mukamel, and T. Scopigno, "On the resolution limit of femtosecond stimulated Raman spectroscopy: Modelling fifth-order signals with overlapping pulses," ChemPhysChem **16**(16), 3438–3443 (2015).

[31] B. K. Agarwalla, H. Ando, K. E. Dorfman, and S. Mukamel, "Stochastic Liouville equations for femtosecond stimulated Raman spectroscopy," J. Chem. Phys. **142**(2), 024115 (2015).

[32] H. Ando, B. P. Fingerhut, K. E. Dorfman, J. D. Biggs, and S. Mukamel, "Femtosecond stimulated Raman spectroscopy of the cyclobutane thymine dimer repair mechanism: A computational study," J. Am. Chem. Soc. **136**, 14801 (2014).

[33] S. Mukamel and S. Rahav, "Ultrafast nonlinear optical signals viewed from the molecule's perspective: Kramers–Heisenberg transition-amplitudes versus susceptibilities," in *Advances in Atomic, Molecular, and Optical Physics*, edited by E. Arimondo, P. R. Berman, and C. C. Lin (Academic Press, 2010), Vol. 59, Chap. 6, pp. 223–263.

[34] R. Kubo, "Stochastic Liouville equations," J. Math. Phys. **4**(2), 174–183 (1963).

[35] D. M. Jonas, "Two-dimensional femtosecond spectroscopy," Annu. Rev. Phys. Chem. **54**(1), 425–463 (2003).

[36] D. S. Lemons, *An Introduction to Stochastic Processes in Physics* (The Johns Hopkins University Press, 2002).